

MSc Biomedical Engineering

Thesis

Estimation of Knee Joint Kinetics using IMUs and Physics-Informed Machine Learning during Walking and Single-Leg Hop tests in ACLR Rehabilitation



Gijs Hofste

July, 2025

Supervisors:

dr. ir. B. J. F. van Beijnum

ir. S. Krishnakumar

dr. E. H. F. van Asseldonk

Department of Biomedical Signals and Systems

Faculty of Electrical Engineering,

Mathematics and Computer Science,

University of Twente

UNIVERSITY OF TWENTE.

Contents

Abstract	3
1 Introduction	4
2 Materials and methods	6
2.1 Dataset	6
2.2 Data processing pipeline	8
2.3 Physical loss function	12
2.4 Model frameworks and evaluation	13
2.5 Model development	15
2.6 Statistical analysis	16
3 Results	17
3.1 Estimation performance of PINN and baseline FNN during walking	17
3.2 Estimation performance of PINN and baseline FNN during SLH	19
3.3 Target knee kinetics within each cohort	21
3.4 Effects of training data size	23
3.5 Effects of physical loss weight	24
4 Discussion	25
4.1 Overall comparison	25
4.2 Evaluation on estimated kinetic variables	25
4.3 Movement complexity and inter-subject variability	26
4.4 Training data size and physical loss weighting	27
4.5 Limitations	27
4.6 Clinical implications	28
4.7 Future research	28
5 Conclusion	29
A Declarations	34
B Data processing pipeline	35
C Estimation performance per fold	38
D Target knee kinetics	40
E Evaluation of input variables	43

Abstract

Evaluation of knee joint loading is essential for monitoring recovery and supporting return-to-sport (RTS) decisions following anterior cruciate ligament reconstruction (ACLR). This study investigates the estimation of three-dimensional knee joint kinetics from inertial measurement unit (IMU) data using a physics-informed neural network (PINN) during walking and single-leg hop tests.

A data processing pipeline was developed to align and generalize inertial and optical motion capture data. Segment kinematics derived from IMUs were used as input to estimate knee joint kinetics, while enabling three-dimensional inverse dynamics through rigid-body modeling. An adaptable neural network framework was designed to incorporate physical constraints via a loss function based on three-dimensional segment-based inverse dynamics.

The PINN was compared to a baseline data-driven model to evaluate prediction performance. While the physical constraints supported biomechanical interpretable estimations, the PINN did not outperform the baseline model. Both models showed reduced accuracy for kinetic components with lower magnitudes, particularly in the mediolateral direction. Moreover, no consistent improvements were found under limited data conditions or varied physical loss weighting. These findings suggest that physical constraints may not enhance performance when data quantity or consistency is insufficient.

Despite these limitations, this study provides a methodological basis for future research on IMU-based kinetic estimation in ACLR rehabilitation. Further development is needed to improve model accuracy and robustness. With sufficient performance, such models could enable subject-specific assessments of limb asymmetry and support RTS decision-making, ultimately reducing the risk of reinjury.

1 Introduction

Anterior cruciate ligament (ACL) tears are among the most common knee injuries, particularly in sports, with an estimated incidence of 120,000 cases annually in the United States [1, 2]. The ACL plays an essential role in stabilizing the knee joint by preventing anterior translation of the tibia relative to the femur and by limiting hyperextension [2–4]. Excessive knee hyperextension or rotational loading, often occurring during sports, can result in ACL rupture. Due to the ligament's limited healing capacity and the resulting knee instability, ACL reconstruction (ACLR) is often required to restore knee function [3, 5]. The primary goal of ACLR is to enable patients to safely return to their preinjury activity levels, usually referred to as return to sports (RTS) [4–7]. Reconstruction typically involves replacement of the ligament with a graft harvested from the hamstring tendon, patellar ligament or quadriceps tendon [5].

Over the years, several goal or criteria based guidelines have been developed for ACLR rehabilitation [1, 2, 8, 9]. These guidelines involve multiple phases, in which patients recover from surgery, improve strength, and enhance neuromuscular control to ultimately return to their preinjury activity level [10]. Throughout this process, clinicians rely on functional performance tests that provide objective, reliable and valid outcomes for knee quality assessment [8].

Walking assessments are commonly included, as asymmetrical walking patterns have been reported in patients who fail RTS criteria [1, 11, 12]. In particular, significant differences in knee joint kinetics have been found between the injured and contralateral limb during walking, even in later phases of rehabilitation [12–14]. These include reduced peak knee extension and flexion moments, and altered GRFs. In addition, the single-leg hop for distance (SLH) is one of the most frequently used RTS tests. This test allows for reliable comparison between injured limb and contralateral healthy limb [8]. Previous studies have shown significant differences in knee kinetics between the injured and contralateral limbs during SLH [8, 15, 16]. These include reduced knee joint moments, particularly in the sagittal plane, and lower vertical GRFs on the injured limb.

Notably, these kinetic asymmetries have been observed months after surgery, even in ACLR patients who meet criteria for RTS [12, 17]. This indicates that traditional performance tests may underestimate the presence of neuromuscular deficits. The observed kinetic alterations reflect compensatory movement patterns, which may increase the risk of reinjury or delayed recovery, a concern emphasized by Gokeler et al. [7]. The authors further reported that only 65% of patients return to their preinjury level of sports, and that current RTS assessments fail to identify those at increased risk of reinjury [7]. Therefore, quantitative movement analysis provides a way to enhance decision-making for RTS during ACLR rehabilitation, by enabling more objective evaluation of joint loading [6, 18].

Optical motion capture (OMC) systems, in combination with force plates (FPs), are considered the gold standard for quantitative movement analysis [13, 14, 17, 19–22]. These system enable the assessment of joint loading, reflected in three-dimensional joint reaction forces and net joint moments [19, 20]. However, this approach contains several downsides, including lab dependency, costs, and extensive time for preparation. In the context of ACLR rehabilitation, on-field measurements in a sport-related environment are essential to support decision making for RTS, preferring lab independent assessment [6, 21]. Due to their cost-effectiveness, portability and ability to monitor on-field, inertial measurement units (IMUs) offer a promising alternative for quantitative motion analysis outside the lab [23]. Inertial motion capture (IMC) systems integrate multiple IMUs toe estimate full-body kinematics. Commercial IMC systems such as Xsens MVN (Xsens, Enschede, the Netherlands) have shown good agreement with OMC systems in terms of joint angle estimation [21]. This makes them a practical tool for monitoring kinematic recovery during ACLR rehabilitation in on-field settings. However, IMUs cannot directly measure external kinetics at the ground interface, such as ground reaction forces (GRFs) and ground reaction moments (GRMs), which are essential for estimating joint reaction forces and net joint moments [19, 20]. Therefore, computational methods are needed to obtain these kinetic parameters.

Machine learning (ML) approaches have shown promise for estimating joint kinetics without direct GRF or GRM measurements [24]. For instance, Stetter et al. [25] investigated the estimation of knee joint forces (KJFs) using a ML approach during relevant movements, such as walking and SLH. The authors showed promising performance of a feedforward neural network (FNN) in estimating KJFs based on data from two IMUs. However, they reported reduced prediction accuracy for the mediolateral (M-L) force components, likely due to their relative low magnitude. In such cases, small

absolute errors can have a large effect on the accuracy of the output estimates. This limitation is critical in the context of ACLR, where accurate assessment of three-dimensional joint loading is essential to support decision-making.

To address these challenges, a promising approach is to constrain ML model outputs through biomechanical or physical principles. Hybrid models that integrate both data-driven learning and biomechanical constraints have shown potential for improving prediction robustness and interpretation, particularly for level walking and running in healthy cohorts [26–28]. Building on this concept, a class of hybrid models called physics-informed neural networks (PINNs) has recently been introduced [29, 30]. PINNs incorporate known differential equations that represent underlying physiological mechanisms directly into the training of a neural network. This incorporation allows the model to satisfy both data-driven as well as physical interpretation. By embedding physical constraints such as inverse dynamics, PINNs are able to learn and regularize interpretable movement patterns even from sparse datasets [30, 31]. Notably, Stetter et al. [25] also identified limited training data as a key limitation on model performance. This further highlights the relevance of PINNs in biomechanical applications where obtaining large, high-quality datasets is difficult. This is particularly relevant in the context of ACLR rehabilitation, where data collection is often limited due to small sample sizes and inter-subject variability [7, 8]. In such cases, the ability of PINNs to generalize from limited data while incorporating biomechanical interpretation makes them a promising tool for supporting decision-making.

This study focuses on establishing model performance of a PINN in estimating knee kinetics for healthy control limbs and injured limbs within the context of ACLR rehabilitation. While analysis of limb symmetry in ACLR patients is clinically important, it is beyond the scope of this work. Establishing robust and accurate estimation models for these distinct cohorts is a necessary step before extending the approach to more complex, subject-specific asymmetry analyses.

Hence, the research question of this study is defined as follows:

How does incorporation of three-dimensional inverse dynamics influence the estimation of three-dimensional knee joint kinetics from IMU data using a PINN during walking and single-leg hop tests in the context of ACLR rehabilitation?

It is hypothesized that the use of the PINN approach will enhance the estimation performance of kinetic components with relatively low magnitudes through improved physical interpretation, compared to a baseline data-driven neural network. Furthermore, these advantages are expected to be most noticeable when training data is limited.

To answer the research question, the following sub-questions in this study are defined:

- How can raw IMC and OMC data be spatiotemporal aligned and generalized?
- How can segment kinematics be obtained from IMU data in a way that (1) mimics the Xsens MVN biomechanical model for use as input to a neural network, and (2) enables three-dimensional inverse dynamics for rigid-body segments to support physical loss computation?
- How can three-dimensional inverse dynamics be implemented into neural network development to support biomechanical interpretable estimations?
- How can an adaptable neural network framework be designed to incorporate biomechanical constraints, including a physical loss function based on three-dimensional inverse dynamics?

2 Materials and methods

In Section 2.1, the details of the dataset used in this study are presented. In Section 2.2, the data processing steps are presented and discussed. Part of the processed data is necessary for the formulated physical loss function, explained in Section 2.3. Further, the processed data as well as the formulated physical loss function are used for developing various models using the adaptable framework presented in Section 2.4. The development of each model is done through a developed deep learning approach, which is explained in Section 2.5. In Section 2.6, a number of performance metrics are discussed for evaluating the quality of the various developed models.

2.1 Dataset

The dataset contains two participant populations: healthy control subjects and ACLR patients. Subject characteristics are given in Table 1.

Table 1. Overview of subject characteristics. Mean \pm standard deviation (SD) values are shown.

Characteristic	Healthy control subjects (n = 9)	ACLR patients (n = 8)
Gender (M/F)	3/6	2/6
Body height (cm)	173.6 \pm 7.8	173.2 \pm 9.4
Body mass (kg)	70.5 \pm 8.9	72.5 \pm 17.7
Injury leg (L/R)		2/6
Time since surgery (months)		8.8 \pm 2.8
Time since start rehabilitation (months)		8.0 \pm 2.8

Participants were monitored in the Movement Lab of Roessingh Research and Development (Enschede, the Netherlands). This lab contains an eight-camera OMC system (VICON, Oxford, UK), connected and configured with two embedded FPs (OR6-5-1000, AMTI, Watertown, MA, USA). Besides, the lab has an IMC system consisting of MTw Awinda IMUs (Xsens, Enschede, the Netherlands).

Prior to the actual measurements, reflective markers and IMUs were placed and fixated on the participants, as illustrated in Figure 1. Following the instruction of the OMC system, a total of 30 reflective markers were placed on bony landmarks [19]. Additionally, a total of eight IMUs were placed across the lower body and sternum following the recommended locations [23]. Hence, each IMU was mounted on a fabricated flat plastic rig containing a cluster of three additional reflective markers [32]. This rig provides a possibility for spatiotemporal alignment between the IMC and OMC systems.

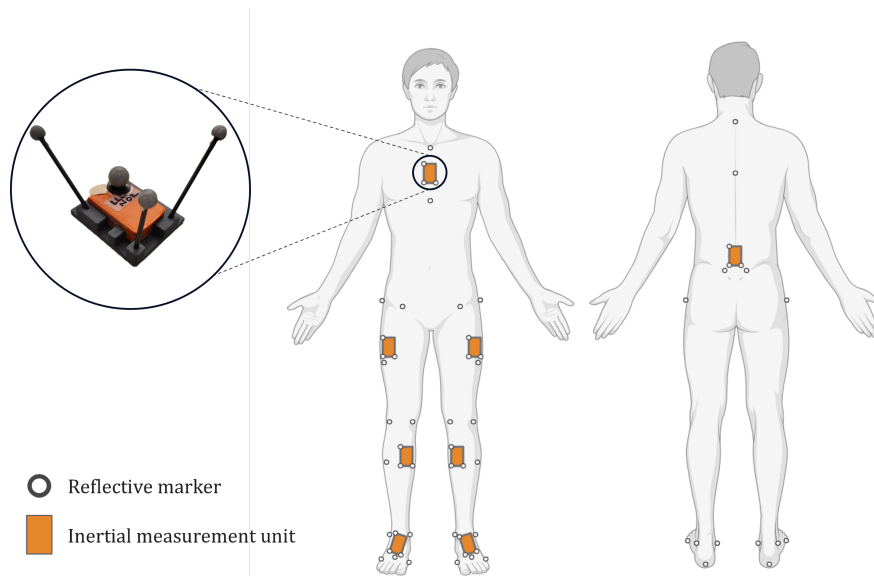


Figure 1. Anterior and posterior view of measurement setup, including reflective markers and IMUs placed across lower body and sternum [19, 23]. IMUs were mounted on a rig, containing additional reflective markers [32]. Created with BioRender.com.

After placement and fixation of the necessary markers and sensors, participants were instructed to perform necessary calibration tasks, including (static) N-pose and segment-specific movement. The latter includes spinal bending, knee bending and toe tipping, each for five repetitions. Subsequently, after familiarization, participants performed two successful trials of walking and SLH (per leg). The trial was deemed to be successful when correct foot placement on the embedded FPs was achieved.

During the successful trials, trajectories of the reflective markers were recorded at 100 Hz using four Vero 2.2 MP cameras and four Vantage 5 MP cameras (VICON, Oxford, UK). Additionally, both FPs collected analog GRFs and GRMs at 1000 Hz, temporally aligned with the marker trajectories. During immediate post-processing, the Plug-in Gait (PiG) model is applied to achieve target kinetics sampled at 100 Hz, including digital GRFs, joint reaction forces, and net joint moments [19]. Raw accelerometer, gyroscope, magnetometer data of the IMUs have been recorded at 40 Hz using MT Manager (Xsens, Enschede, the Netherlands). The IMU data also includes quaternions, describing the orientation of the sensors over time.

For the purpose of this study, the dataset was divided into two cohorts: (1) healthy limbs, represented by non-injured limbs of healthy control subjects, and (2) injured limbs, represented by the ACLR-affected limbs. Importantly, the contralateral (non-injured) limbs of ACLR patients were not included in the healthy cohort. This exclusion was implemented to ensure that the healthy cohort reflected truly unaffected movement patterns, thereby avoiding possible confounds introduced by compensatory strategies known to persist in non-injured limbs during ACLR rehabilitation [12, 16]. While inter-limb comparisons within ACLR patients are clinically relevant, such analyses was considered beyond the scope of the current study.

2.2 Data processing pipeline

The dataset contains several data files associated with successful walking and SLH trials of all participants. For each trial, motion files from the OMC+FP system (c3d-file) as well as from each individual IMU (txt-file) are present. To address the sub-question concerning spatiotemporal alignment and generalization of data from both systems, various processing steps are applied to each trial. These include: Collect data, prepare data, spatiotemporal alignment, segment motion and normalization. An overview of these steps is provided in Figure 2. A more detailed overview is provided in Figure B.1 (see Appendix B). All processing steps described in this section were done in MATLAB R2024a (Mathworks, Inc., Natick, MA, United States).

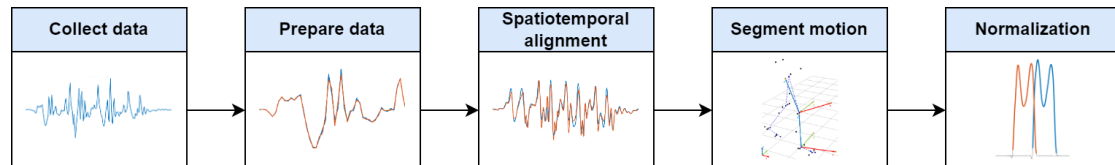


Figure 2. Overview of data processing steps applied to each trial.

Collect data and prepare data

Motion files associated to each trial were initially imported. Reflective marker trajectories, target kinetics and sensor kinematics were filtered using a third-order zero-phase (non-causal) low pass Butterworth filter with a cut-off frequency of 15 Hz, in order to prevent distortion of the data by high-frequency noise [25]. For obtaining true kinematic motion, gravity component removal was applied to each IMU. This was achieved by subtracting the average linear acceleration in vertical direction, measured during static periods of the trial. Angular acceleration of the IMUs and linear accelerations of the markers were determined, which was required for further steps. To obtain these accelerations, differentiation was applied using the central difference scheme. Due to the possibility of gaps present during static periods of the trial, only the data during dynamic period was included. The dynamic period was extracted based on the linear acceleration of the ankle joint.

Spatiotemporal alignment

In order to compare data from both systems, it is necessary to align them both in spatial and temporal domains to ensure that measurements correspond to the same locations and time points. All data in this study was processed at 100 Hz, matching the sampling rate of the target kinetics derived from the PiG model. The IMU data was resampled to 100 Hz in order to match the sampling frequency of the target data, required for synchronization. Accelerometer and gyroscope data have been resampled using linear interpolation, whereas quaternion data was resampled using spherical linear interpolation (SLERP) [33, 34]. To align with the global spatial configuration of the OMC system, a heading reset was applied to the IMU data (see Figure B.2 in Appendix B) [32, 35, 36]. Here, it was assumed that participants moved primarily in the anterior-posterior or x-direction, as defined by the OMC system. Heading directions in the transverse or xy-plane, for both the optical and inertial motion data, were estimated using principal component analysis (PCA). This was done to determine the heading difference in xy-plane of the global reference frame for each IMU with respect to the global reference frame, defined by the OMC system. As both IMC and OMC systems align in vertical or z-direction, the heading difference was represented by the angle around this direction (yaw). Specifically, this heading difference was subsequently calculated as the yaw angle between the principal axis derived from the global linear acceleration of the IMU and the principal axis derived from one of the reflective markers of the associated rig. To achieve precise temporal alignment between both systems, cross-correlation was employed (see Figure B.3 in Appendix B) [27, 32]. Specifically, the norm of the acceleration recorded by the IMU positioned on the right thigh was computed and compared to the corresponding acceleration derived from the one of the reflective marker from the corresponding rig. By identifying the time lag through cross-correlation, the temporal offset was adjusted by trimming the lagging portion. To ensure both datasets covered an identical time span, the longer sequence was subsequently truncated. If no sufficient alignment was achieved, the procedure stopped and the trial was excluded from further processing and analysis. This sufficient alignment was defined by an excellent correlation ($r > 0.90$) [37].

Segment kinematics and kinetics

To accurately represent true body motion in accordance with the anatomical spatial configurations of body segments, sensor-to-segment alignment was applied to the IMU data [20, 23]. This alignment process involves both a translational shift from the sensor location to the relevant anatomical origin and a rotational transformation from the local sensor frame to the local segment frame. To enable these transformations, an additional reflective marker mounted on the associated rig was used to indicate the sensor location, as this information is not directly available from the IMU data. Additionally, the PiG model provides virtual marker trajectories that represent joint centers and the orientations of local segment axes. Each segment includes four virtual markers defined within its local segment frame: at the origin, along the anterior axis, the proximal (longitudinal) axis, and the lateral axis. The origin marker corresponds to the center of the distal joint, while the proximal marker represents the center of the proximal joint. A representative visualization of the joint centers and local segment axes is provided in Figure 3.

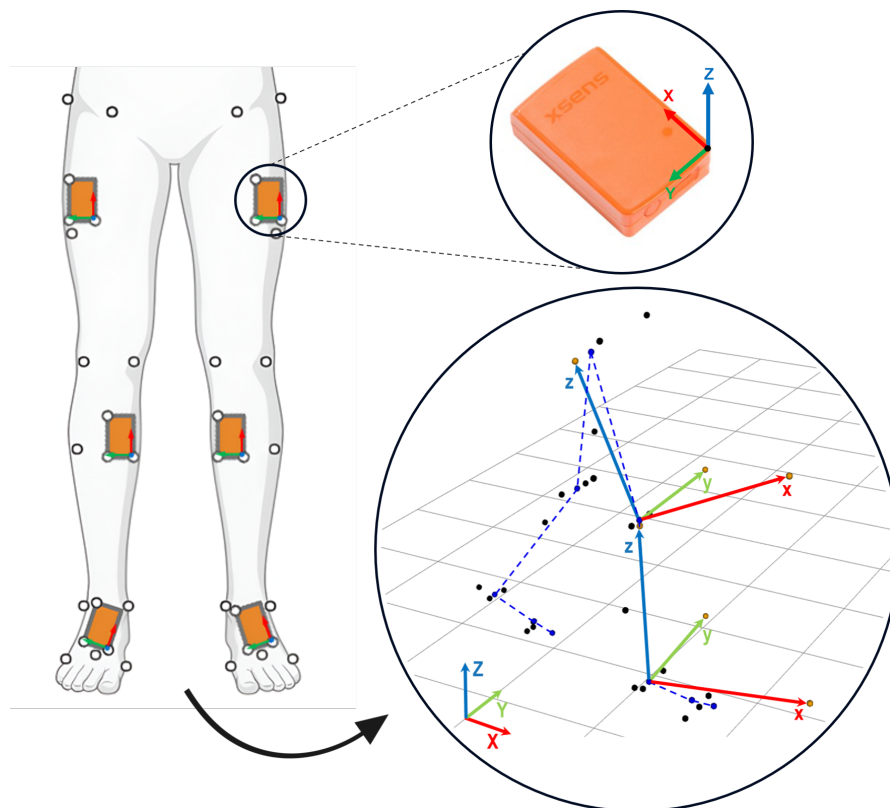


Figure 3. Visualization of local sensor axes and representative local segment axes present in the measurement setup. Virtual markers represent joint centers and the orientations of local segment axes: Origin marker (blue dot) and markers along anterior, proximal and lateral axis (orange dot). Orientations of the segment axes (right thigh and shank) are defined by components x (red arrow), y (green arrow) and z (blue arrow). Created with BioRender.com.

To address the sub-question concerning the estimation of segment kinematics and their use in three-dimensional inverse dynamics, two distinct sensor-to-segment alignment approaches were applied in this study. These approaches serve different roles within the adaptable neural network framework.

In the first approach, sensor data was translated to the proximal joint center of the corresponding segment and rotationally transformed to align with the global reference frame. This approach mimics the segment reference frames used in the Xsens MVN biomechanical model [23] and provides the input kinematics to the neural network. In contrast, the second approach translates the sensor data to the center of mass (COM) of the associated segment and rotationally transformed into the local segment frame [20, 38]. The COM location was estimated based on segment length calculated from the positions of the proximal and distal joint centers, and scaled using segment-specific COM ratios reported by de Leva [39]. This second approach is essential for enabling three-dimensional inverse dynamics calculations for a segment, used to support physical loss computation [20, 38].

Both sensor-to-segment alignment approaches are illustrated in Figure 4.

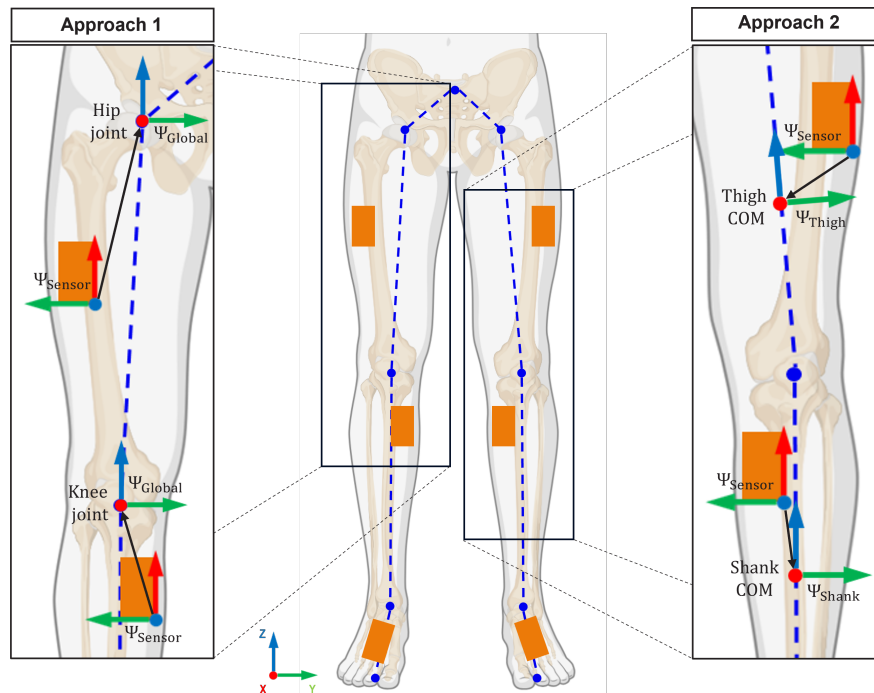


Figure 4. Sensor-to-segment alignment applied in two distinct ways. Approach 1 (left) translates sensor location to the segment's proximal joint center and rotationally transforms to align with the global reference frame (Ψ_{Global}). Approach 2 (right) translates to the segment's COM and rotationally transforms to the local segment frame (e.g. Ψ_{Thigh} and Ψ_{Shank}). Created with BioRender.com.

To apply the three-dimensional inverse dynamics, kinetic data at both segment extremities are required [20, 38]. The PiG model provides joint kinetics expressed in the distal segment axes, representing the kinetics at the proximal end of the segment [19]. To obtain the kinetics at the distal extremity, joint forces and moments of the associated distal joint were rotationally transformed into the local segment frame using the virtual markers.

Normalization

For generalization and interpretation, kinetic data was normalized to the body anthropometrics of the participants, as body mass (and weight) has shown to explain a significant amount of the variance during walking [25, 40, 41]. Specifically, forces were normalized to the bodyweight (BW), while moments were normalized to both BW and bodyheight (BH). Subsequently, kinematic and kinetic data components were adjusted to use standardized anatomical terminology, allowing for generalization across both limbs. Components were adjusted to represent linear and angular motion in or around anterior-posterior (A-P), medial-lateral (M-L), and vertical (V) directions.

Additionally, both kinematic and kinetic data were normalized over time for both walking and SLH[25]. Time normalization was achieved through segmentation based on GRFs, with specific event points identified depending on the movement type. For walking, heel strike and toe-off events were identified using a contact-threshold of 20 N [25]. Since only two embedded FPs were available, each foot could be measured independently, and consequently, only the stance phase was captured for each limb. For hopping, four key events were identified: initial push-off, end push-off, initial landing, and end of landing. These events were identified using a combination of the contact-threshold of 20 N, local maxima in the vertical GRF signal, and the associated peak knee flexion angle [25, 42].

Finally, kinematic and kinetic variables for each segment were organized into structured datasets and saved separately based on the associated limb. For limb-independent segments, such as the pelvis and sternum, separate datasets were generated for each limb-specific trial, aligned to the timing of the corresponding limb. An overview of the variables included in the structured datasets is given in Table 2.

Table 2. Dataset variables with their corresponding unit and definition. Segments i include sternum, pelvis, thigh, shank and foot. BW = bodyweight, BH = bodyheight.

Variable	Unit	Definition
t	%	Normalized time as percentage of movement.
m	kg	Body mass.
l	m	Body height.
l_i	m	Segment length.
${}^G\vec{a}_{i_p}(\hat{t})$	m/s^2	Linear acceleration vector of segment i over time of movement, expressed in the global reference frame G with the origin at the proximal joint.
${}^{B_i}\vec{a}_{i_{COM}}(\hat{t})$	m/s^2	Linear acceleration vector of segment i over time of movement, expressed in the local segment frame B_i with the origin at the COM.
${}^{B_i}\vec{\omega}_i(\hat{t})$	rad/s	Angular velocity vector of segment i over time of movement, expressed in the local segment frame B_i .
${}^{B_i}\vec{\alpha}_i(\hat{t})$	rad/s	Angular acceleration vector of segment i over time of movement, expressed in the local segment frame B_i .
${}^{B_i}\vec{F}_{i_p}^*(\hat{t})$ or ${}^{B_i}\vec{F}_i^*(\hat{t})$	BW	Normalized force vector of segment i over time of movement, expressed in the local segment frame B_i with the origin at the proximal joint. This also represents the normalized joint force.
${}^{B_i}\vec{F}_{i_d}^*(\hat{t})$	BW	Normalized force vector of segment i over time of movement, expressed in the local segment frame B_i with the origin at the distal joint.
${}^{B_i}\vec{M}_{i_p}^*(\hat{t})$ or ${}^{B_i}\vec{M}_i^*(\hat{t})$	$BW \cdot BH$	Normalized moment vector of segment i over time of movement, expressed in the local segment frame B_i with the origin at the proximal joint. This also represents the normalized joint moment.
${}^{B_i}\vec{M}_{i_d}^*(\hat{t})$	$BW \cdot BH$	Normalized moment vector of segment i over time of movement, expressed in the local segment frame B_i with the origin at the distal joint.
${}^G\vec{GRF}^*(\hat{t})$	BW	Normalized ground reaction force vector over time of movement, expressed in the global reference frame G with the origin at the center of the FP.
${}^G\vec{GRM}^*(\hat{t})$	$BW \cdot BH$	Normalized ground reaction moment vector of segment i over time of movement, expressed in the global reference frame G with the origin at the center of the FP.

2.3 Physical loss function

To address the sub-question concerning the implementation of three-dimensional inverse dynamics into the development of a neural network estimation, a physical loss function was formulated. This physical loss captures discrepancies in three-dimensional translational and rotational dynamics of lower limb's rigid-body segments. The translational and rotational dynamics were represented by Newtonian and Euler's three-dimensional equations of motion for a segment, following Section 7.4 in the work of Winter [20]. In this study, the physical loss was applied to the thigh and shank segments, as the focus is on knee kinetics.

For the translational dynamics, the normalized net force acting on segment i , denoted as $\sum \vec{F}_i^*$, included components in A-P, M-L and V direction. The vectorized equation of motion governing the three-dimensional translational dynamics was transformed to the following loss function:

$$\sum \vec{F}_i^*(t) = {}^{B_i} \vec{F}_{i,p}^*(t) - {}^{B_i} \vec{F}_{i,d}^*(t) - \frac{\zeta_i}{g} {}^{B_i} \vec{a}_{iCOM}(t) = L_{translational,i} \quad (1)$$

This expression includes the normalized forces and the linear acceleration corresponding to the segment (see Table 2). The term ζ_i denotes the mass ratio of segment i with respect to the body mass, while g denotes the gravitational acceleration.

For the rotational dynamics, the normalized net moment acting on segment i , denoted as $\sum \vec{M}_i^*$, includes the components in A-P, M-L and vertical (V) direction. The vectorized equation of motion governing the three-dimensional rotational dynamics was transformed to the following loss function:

$$\begin{aligned} \sum \vec{M}_i^*(t) = & \frac{\zeta_i l_i^2}{gl} \begin{bmatrix} k_{i,A-P}^2 \\ k_{i,M-L}^2 \\ k_{i,V}^2 \end{bmatrix} {}^{B_i} \vec{\alpha}_i(t) + \\ & \frac{\zeta_i l_i^2}{gl} \begin{bmatrix} k_{i,V}^2 - k_{i,M-L}^2 & k_{i,V}^2 - k_{i,M-L}^2 & 0 \\ 0 & k_{i,A-P}^2 - k_{i,V}^2 & k_{i,A-P}^2 - k_{i,V}^2 \\ k_{i,M-L}^2 - k_{i,A-P}^2 & 0 & k_{i,M-L}^2 - k_{i,A-P}^2 \end{bmatrix} {}^{B_i} \vec{\omega}_i(t) - \\ & \frac{1}{l} \begin{bmatrix} -\delta_{i,p} l_i & 0 & 0 \\ 0 & 0 & \delta_{i,p} l_i \\ 0 & 0 & 0 \end{bmatrix} {}^{B_i} \vec{F}_{i,p}^*(t) + \frac{1}{l} \begin{bmatrix} -\delta_{i,d} l_i & 0 & 0 \\ 0 & 0 & \delta_{i,d} l_i \\ 0 & 0 & 0 \end{bmatrix} {}^{B_i} \vec{F}_{i,d}^*(t) + \\ & {}^{B_i} \vec{M}_{i,p}^*(t) - {}^{B_i} \vec{M}_{i,d}^*(t) = L_{rotational,i} \end{aligned} \quad (2)$$

This expression includes the normalized forces, normalized moments, angular acceleration, angular velocity, body height, and segment length corresponding to the segment (see Table 2). The term ζ_i denotes the mass ratio of segment i with respect to the body mass, g denotes the gravitational acceleration, and $k_{i,A-P}$, $k_{i,M-L}$, and $k_{i,V}$ denote the radii of gyration ratios associated with anteroposterior (A-P), mediolateral (M-L), and vertical (V) direction, respectively. The terms $\delta_{i,p}$ and $\delta_{i,d}$ denote the segment ratios for the distance between the segment's center of mass and the proximal (p) and distal (d) ends of the segment, respectively, with respect to the segment length.

Summation of the applied loss functions in Equation 1 and Equation 2 to both thigh and shank, gives the following physical loss function:

$$L_{physical} = \sum_{i=thigh,shank} L_{translational,i} + L_{rotational,i} \quad (3)$$

2.4 Model frameworks and evaluation

In this study, an adaptable custom framework is designed which allows development of a model through either or both data-driven and physical interpretation, such as the PINN. Several models have been developed and evaluated using the custom framework to assess the prediction performance on the estimation of knee joint and ground reaction kinetics based on segment kinematics. The custom framework and models were made in Python 3.9.7 (Python Software Foundation, Wilmington, DE, United States) using the PyTorch package (version 2.4.1) [43].

In this study, a FNN architecture was developed for the PINNs, containing an input layer, several hidden layers, and an output layer. The model is developed using both data-driven and physics-informed (PI) constraints. Input variables include linear accelerations and angular velocities of the pelvis, thighs, shanks and feet. The output variables consists of normalized joint forces and moments at the hip, knee, and ankle, as well as normalized ground reaction forces and moments. These variables are given in Table 2 in Section 2.2.

A PI layer is incorporated into the PINN architecture to enable physical interpretation in estimations. This layer utilizes the input kinematics, predicted kinetics and additional variables, such as angular velocities, individual segment lengths, and body height to compute the physical loss (see Section 2.3). An overview of the complete PINN framework is illustrated in Figure 5.

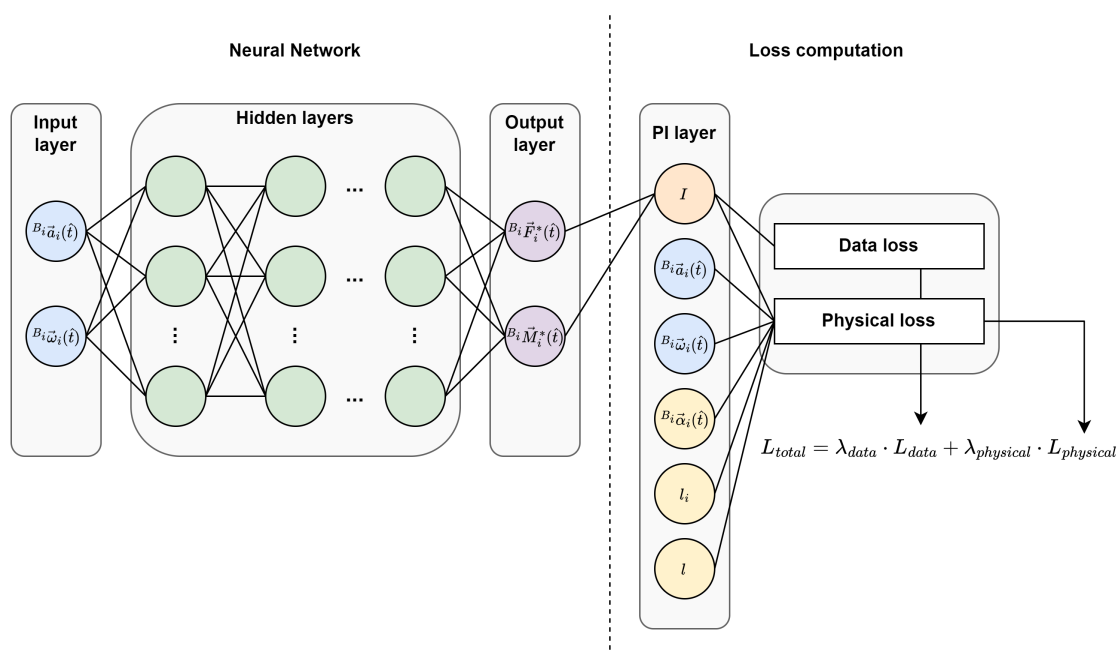


Figure 5. Overview of PINN framework, consisting of two main components: a neural network and a loss computation compartment. The neural network includes an input layer, several hidden layers, and an output layer, mapping segment kinematics to joint and ground reaction kinetics. The loss computation compartment contains a PI layer, which incorporates the variables necessary for computing both the data loss and the physical loss. The individual losses are weighted (λ) and summed to compute the total loss.

PINNs were developed and evaluated across several movement scenarios: walking in healthy cohort, walking in injured cohort, SLH in healthy cohort, and SLH in injured cohort. For every scenario, model evaluation followed a leave-one-subject-out cross-validation (LOSO CV) approach [25, 27]. In each fold, data from one subject was held out as unseen test-data, while the data from the remaining subjects was used to train the model. This process was repeated until each subject had been used as a test-subject once. This enables assessment of the model's generalization performance across subjects. This LOSO CV approach is illustrated in Figure 6.

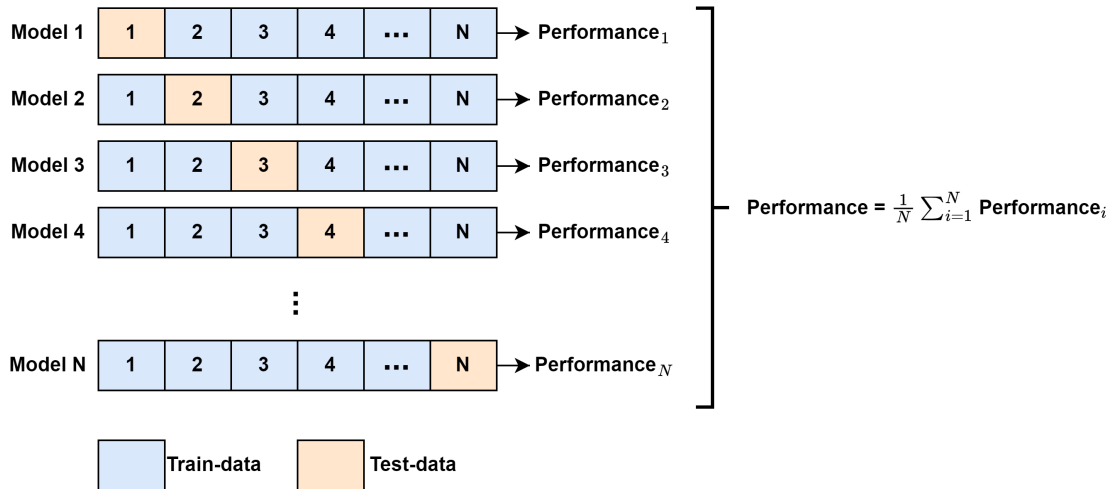


Figure 6. The LOSO CV approach consists of multiple folds, where in each fold a model is trained on data from all but one subject and tested on the data from the held-out subject. The average performance across all folds is used to assess the model's generalization capability.

To investigate the influence of incorporating three-dimensional inverse dynamics on knee joint kinetics estimation, the performance of the PINNs was compared to a baseline model. This baseline consisted of a FNN with the same development and evaluation approach as the PINN, but without the physical constraints. In other words, the baseline FNN was developed solely using data loss, omitting the PI layer and the physical loss component (see Figure 5). The same LOSO CV procedure was applied to the baseline model for each scenario to ensure a fair comparison of generalized performance.

In addition to the main evaluation, further analyses were conducted to investigate the effects of specific components during development of the PINN model, including: the characteristics of target data, the size of the training data and the weighting of the physical loss term.

To assess the variability in target data, knee kinetics from all individual trials within both healthy and injured cohorts were evaluated. This allowed for inter-subject variability, within each cohort. Considering such variability is essential, as it can impact the robustness and generalization of the model [44, 45]. While differences between healthy and injured cohorts (inter-cohort variability) are acknowledged as important, detailed analysis of these inter-cohort differences is beyond the scope of the current study. This aligns with the study's focus on establishing model performance within each cohort separately before addressing more complex comparative analyses.

The effects of training data size and physical loss weighting were examined within a controlled setting: a single fold of the LOSO CV applied to the healthy cohort during walking (see Figure 6), where the same subject was consistently used as test-data. With this approach, the same subject was consistently used as test-data across all experiments, allowing for a focused comparison of these individual factors while minimizing confounding variability.

To evaluate the effect of training data size, the number of subjects included in the train-data was incrementally increased to 20%, 40%, 60%, 80%, and 100% of the available training subjects. Here, each step builds upon the previous by adding more subjects. This analysis was performed to both the PINN and the baseline FNN to assess whether the expected benefits of the PINN approach become more evident when training data is limited. To evaluate the effect of the physical loss weighting, the weight assigned to the physical loss component was varied across (logarithmic) values of 0.01, 0.1, 1, 10, and 100, while the data loss weight was held constant at 1. As this analysis involves the physical loss component, it was only applied to the PINN.

2.5 Model development

In each fold, the model is developed following an approach consisting of: data partitioning, hyperparameter specification, data preprocessing and formatting, model training, and model evaluation.

Data partitioning

Data is initially divided subject-wise into train-data and test-data, as explained in Section 2.4. The train-data will be used for model training, while the test-data is used for evaluation of the trained model. Subsequently, the train-data is further divided into data for training and validation using split of 80% to 20% of the training subjects, respectively [25].

Hyperparameter specification

Hyperparameters were specified for the development and architecture of the model. These include number of hidden layers, hidden layer sizes, activation function, training epochs, learning rate, batch size, optimizer, the percentage of total variance explained by principle components (PCs), data loss weight, and physical loss weight. The corresponding values are based on literature and can be found in Table 3 [25, 27, 33, 46, 47].

In the designed custom framework, an option for hyperparameter optimization is embedded. With this option included, part of the hyperparameters were optimized using the Optuna package (version 4.3.0), with the objective of minimizing the validation loss across 50 trials [48]. During this optimization procedure, the model is trained and evaluated with varying hyperparameter settings, dependent on a pre-defined range with sampling (see Table 3).

Table 3. Hyperparameter specification, including type, fixed values, and settings for optimization [25, 27, 33, 46, 47]. * : optional for model development.

Hyperparameter	Type	Fixed Value	Optimization	
			Range	Sampling
Number of hidden layers	int	2	1 - 4	uniform
Hidden layer sizes	int	[250, 100]	50 - 250	uniform
Activation function	function	tanh	N/A	N/A
Training epochs	int	1000	N/A	N/A
Learning rate	float (log)	1e-5	1e-5 - 1e-1	log-uniform
Batch size	float	32	N/A	N/A
Optimizer	algorithm	Adam	N/A	N/A
Explained variance by PCs*	float	0.95	0.90 - 0.95	uniform
Data loss weight*	float	1	N/A	N/A
Physical loss weight*	float	1	N/A	N/A

For the main evaluation (see Section 2.4), hyperparameters were optimized if applicable. In the case of the analyses on the effects of training data size and physical loss weighting, the fixed values were applied.

Data preprocessing and formatting

Input variables are initially standardized using Z-score normalization. This step is essential not only to ensure consistent scaling, but also to enable the optional application of a PCA. The PCA was applied to reduce dimensionality of the input space while balancing information preservation by linear combinations of the initial input variables. The variables had contributions to the optimized number of PCs, explaining cumulatively 90 to 95 percent of the total variance (see Table 3) [46, 47]. Thereby, it decreases the risk of overfitting during model training. The application of a PCA is applied in the main evaluation (see Section 2.4), while only the standardization was applied in the case of the analyses on the effects of training data size and physical loss weighting.

Data corresponding to the input layer, output layer, and PI layer (see Figure 5) were stored in a three-dimensional dataset organized on a per-trial basis. In other words, the dataset maintains a trial-wise structure in a three-dimensional space. This three-dimensional dataset is subsequently converted into a PyTorch Tensor, required for model development using PyTorch [43]. For efficient model development, the dataset is further wrapped into a DataLoader, which facilitates batches loading and iteration. During batch creation, sequences were zero-padded to ensure uniform sequence lengths across all trials within each batch. Simultaneously, a corresponding mask layer was generated using a custom collate function. This mask identified the padded elements and ensured they were excluded from subsequent calculations, preserving data integrity during training.

Model training

Models were trained for 1000 epochs with a batch size of 32, using the adaptive moment estimation (Adam) optimizer implemented in PyTorch (see Table 3). Within each epoch, the model is trained by iteration across all batches. Within each batch iteration, values associated to the batch were extracted from the DataLoader, and output variables were scaled using Z-score normalization to ensure equal contribution to the learning process. A forward pass was initiated to predict the output values using the current model's weights and biases. With the predicted output values, the training loss was computed and subsequently used by the optimizer to update the model's weights and biases through backpropagation and gradient descent [27]. For the data-loss (see Figure 5), the mean-squared-error (MSE) between target and predicted values was used, which is standard practice in regression tasks [25, 27, 33]. Besides, in cases of using the PINN framework, the physical loss was added to the data loss with equal weight of 1, forming a composite loss function. Model performance during epochs was monitored using the validation data, and early stopping was applied if the validation loss did not improve for 100 consecutive epochs. Hence, the validation loss was represented by the MSE between the target and predicted values of the validation data [27].

Model evaluation

The performance of the model was evaluated using the test-data. The predicted output values using the optimized model's weights and biases was initially determined through the forwards pass. Then, the test loss was computed based on the target and predicted values through the data-loss.

2.6 Statistical analysis

Predictive performance of the developed models was assessed by the similarity between the target and estimated output variables (see Section 2.4) using Pearson's correlation coefficient (r). Pearson's r was categorized as weak ($r \leq 0.35$), moderate ($0.35 < r \leq 0.67$), strong ($0.67 < r \leq 0.90$), and excellent ($r > 0.90$) [37, 49]. Additionally, the accuracy of the estimation was assessed using the relative root-mean-squared error (rRMSE) [25, 49]. These performance metrics were averaged across the cross-validation folds to achieve the mean and standard deviation (SD) of the performance.

Furthermore, the performance metrics for the main evaluation (see Section 2.4) were further tested on statistical significance. Specifically, intra-cohort comparisons were made between the performance of the PINN and baseline FNN models, while inter-cohort comparisons were conducted for each model individually. In order to do so, differences between performance metrics were first assessed for normality using the Shapiro–Wilk test ($p < 0.05$). If the normality assumption was satisfied, a paired t -test was conducted to evaluate the statistical significance ($p < 0.05$). In cases where the normality assumption was violated, the non-parametric Wilcoxon signed-rank test was employed instead ($p < 0.05$).

3 Results

In Section 3.1 and Section 3.2, the estimation performance for the main evaluation in this study is presented, involving the comparison of the performance of the PINNs against the baseline FNNs for both healthy and injured cohorts, during walking and SLH, respectively. In Section 3.3, the KJFs used as target for the model development are evaluated across all trials corresponding to healthy and injured cohorts, during walking and SLH. Further, the effects of training data size are presented in Section 3.4. Additionally, in Section 3.5, the effects on the physical loss weighting is presented.

3.1 Estimation performance of PINN and baseline FNN during walking

Figure 7 shows the estimated KJFs during walking for specific cross-validation folds, comparing the PINN and baseline FNN models in both healthy and injured cohorts. In both cases, the models show a moderate ability to follow the target KJFs patterns in the A-P and V directions. However, the estimation of the M-L component remains more challenging, with both models exhibiting reduced accuracy in this direction. Additionally, the estimated KJFs appears smoother for folds corresponding to the healthy cohort compared to those from the injured cohort, suggesting that inter-subject variability may impact the model's predictive performance.

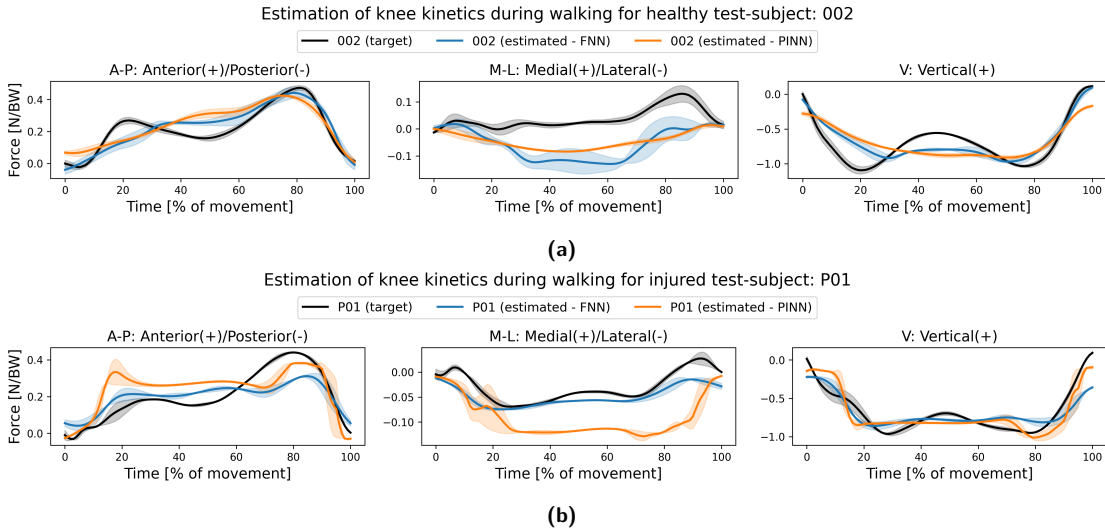


Figure 7. Target (blue) and estimated (orange) KJFs of PINN and baseline FNN models during walking for the cross-validation fold corresponding to test-subject '002' in healthy cohort (a) and test-subject 'P01' in injured cohort (b). Individual trials (thin line), and mean (bold line) and SD (shaded area) across trials are shown.

Figure 8 presents the average Pearson's r and rRMSE values across all cross-validation folds for knee and ground reaction kinetics of both the PINN and baseline FNN models during walking in both healthy and injured cohorts. An overview of the performance per fold is provided in Table C.1 (see Appendix C).

In both cohorts, the PINN and FNN models showed comparable performance for KJFs in the A-P and V directions. Correlation coefficients for these components ranged from 0.43 to 0.95 for the PINNs and 0.66 to 0.88 for the FNNs. Corresponding rRMSE values were also similar, with 15.84%-38.68% (A-P) and 11.55%-36.67% (V) for the PINNs, which had similar ranges for the FNNs. However, performance in the M-L direction was notably lower in both cohorts. Correlation coefficients ranged widely from 0.22 to 0.77 for the PINNs and 0.19 to 0.91 for the FNNs. The rRMSE values in this direction were higher, with PINNs reaching 20.77%-84.09%, reflecting the increased difficulty in predicting this component across both healthy and injured groups.

Performance for KJMs varied across directions. In healthy cohort, the M-L and V directions yielded moderate to strong correlations, ranging from 0.52 to 0.69 (M-L) and 0.52 to 0.87 (V), with corresponding rRMSE values of 23.46%-37.61% (M-L) and 19.76%-43.98% (V). The A-P component showed greater variability, with correlation coefficients ranging from 0.12 to 0.76 and rRMSE values

between 23.34% and 84.35%. In injured cohort, lower correlations and higher rRMSE were obtained for the M-L direction, while the A-P component had increased performance in comparison with the healthy cohort. A statistically significant improvement ($p < 0.05$) in the A-P component was observed in favor of the PINN model in the healthy cohort, whereas the FNN model outperformed the PINN in this same component in the injured cohort. This suggests a possible cohort-dependent variation in model performance for this kinetic variable.

For GRFs, both models exhibited strong performance in the A-P and V directions across cohorts. Correlation coefficients remained high, and rRMSE values were low, indicating accurate predictions. Interestingly, for the M-L component, both models performed better compared to their respective KJF M-L predictions. Correlation coefficients ranged from 0.57 to 0.96, and rRMSE values fell between 9.89% and 35.14%. A statistically significant improvement ($p < 0.05$) in the M-L direction was observed for the PINN model compared to the FNN, highlighting its relative strength in capturing this specific GRF component.

GRMs also showed direction-dependent variation across both cohorts. The A-P direction generally resulted in lower correlation coefficients and higher rRMSE values, consistent with the trends seen in other kinetic variables. In contrast, the M-L and V components performed better overall. A statistically significant deterioration ($p < 0.05$) in the M-L direction was found for the PINN compared to the FNN in both healthy and injured cohort. However, in the injured cohort, the FNN outperformed the PINN in this direction ($p < 0.05$), with the PINN's correlation coefficients ranging widely from -0.45 to 0.94, indicating inconsistent predictions in this group.

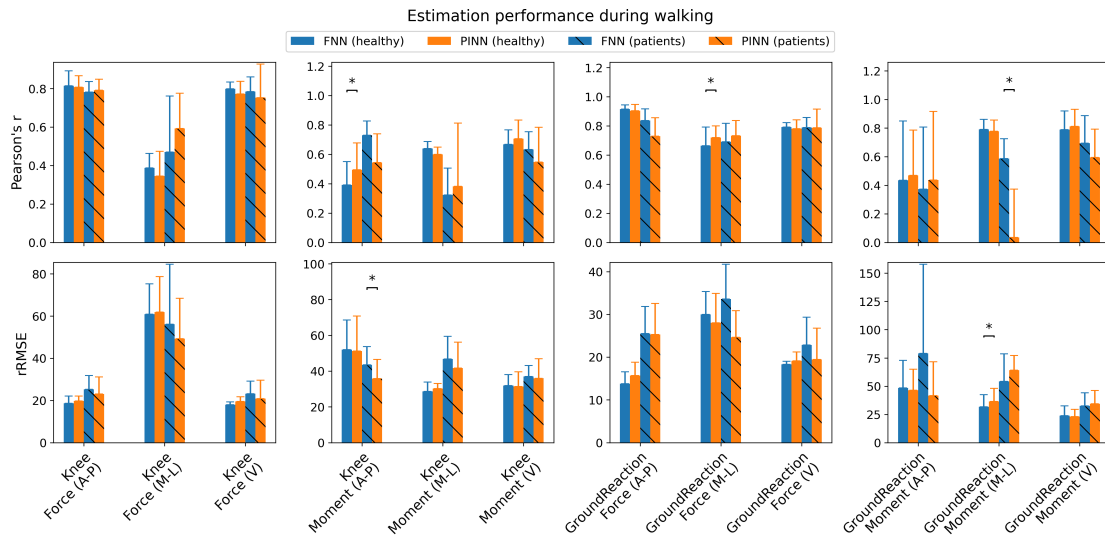


Figure 8. Comparison of Pearson's r correlation and rRMSE values of knee and ground reaction kinetic estimation during walking, between FNN and PINN in healthy and injured cohort. Kinetics include force components and moment around components (A-P = anterior-posterior, M-L=medial-lateral, V=vertical). Data are shown as mean + SD. Statistically significant differences are indicated: $p < 0.05$ (*).

3.2 Estimation performance of PINN and baseline FNN during SLH

Figure 9 shows the estimated KJFs during SLH for the same models and cohorts. In the healthy cohort, both the PINN and baseline FNN models perform well in capturing A-P and V direction KJFs, consistent with walking. However, the M-L component again shows a greater challenge for both models. In the injured cohort, estimation performance further declines, particularly in the A-P and M-L direction. Additionally, the estimated KJFs are visibly less smooth in the fold corresponding to the injured cohort compared to those from the healthy cohort. This reinforces the observation that inter-subject variability introduces increased complexity for model estimation.

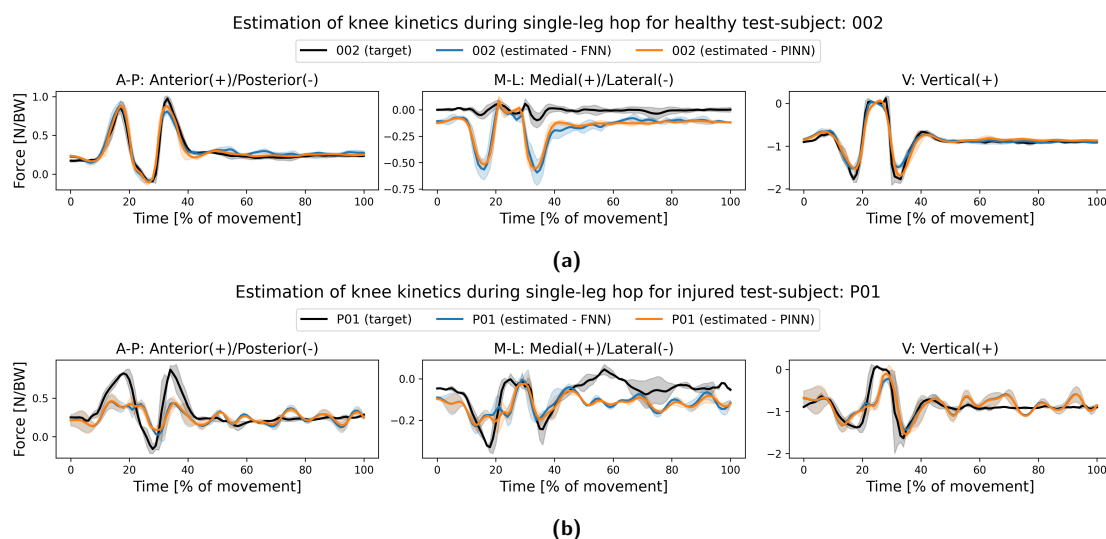


Figure 9. Target (blue) and estimated (orange) KJFs of PINN and baseline FNN models during SLH for the cross-validation fold corresponding to test-subject '002' in healthy cohort (a) and test-subject 'P01' in injured cohort (b). Individual trials (thin line), and mean (bold line) and SD (shaded area) across trials are shown.

Figure 10 presents the average Pearson's r and rRMSE values across all cross-validation folds for knee and ground reaction kinetics of both the PINN and baseline FNN models during SLH in both healthy and injured cohorts. An overview of the performance per fold is provided in Table C.2 (see Appendix C).

In both healthy and injured cohorts, the PINNs and FNNs showed strong and comparable performance in estimating KJFs in the A-P and V directions, consistent with the observations made during walking (see Section 3.1). Correlation coefficients in these directions ranged from 0.40 to 0.96 for the PINNs and 0.48 to 0.95 for the FNNs. Corresponding rRMSE for the PINNs were 5.66%-21.39% (A-P) and 6.64%-19.82% (V), and were similar for the FNNs, indicating high prediction accuracy in these directions across both cohorts. However, as with walking, the M-L component proved more challenging. Correlation coefficients in this direction ranged from -0.54 to 0.76 for the PINNs and -0.40 to 0.82 for the FNNs. The corresponding rRMSE values were substantially higher, with PINNs reaching 15.06%-66.85%. These results underscore the difficulty of accurately estimating the M-L component of KJFs.

For KJMs, the A-P and V components showed moderate performance in both cohorts, with correlation coefficients ranging from -0.14 to 0.73 and rRMSE values between 19.01% and 57.75% across both PINNs and FNNs. These results reflect notable variability in estimation performance across subjects and trials. In contrast, the M-L component exhibited improved performance, particularly in the healthy cohort. Correlation coefficients for this component ranged from 0.34 to 0.88 and rRMSE values were relatively low, ranging from 9.39% to 19.83%. This indicates better model robustness in this direction for healthy subjects. This improved performance may reflect more consistent movement patterns in M-L direction among healthy subjects during SLH, compared to other directions.

For GRFs, both models exhibited strong performance in the V direction across cohorts, aligning with results seen during walking. In the healthy cohort, the A-P component also showed strong performance for both models. However, in the injured cohort, the A-P component was considerably less accurate. Correlation coefficients ranged from -0.10 to 0.43, and rRMSE values increased to

17.06% and 43.25% across PINNs and FNNs. Similar was observed for the M-L component. This reduced accuracy likely reflects altered movement patterns in the injured cohort during SLH. Further, the FNN outperformed the PINN for the A-P direction in terms of rRMSE value ($p < 0.01$).

GRMs were difficult to predict across both cohorts and models, particularly in A-P and M-L directions. Correlation coefficients in these directions were generally low, indicating weak model performance. In the V direction, performance in the healthy cohort was modest, with correlation coefficients ranging from -0.07 to 0.58 across both PINNs and FNNs. However, in the injured cohort, correlation coefficients dropped substantially, ranging from -0.39 to 0.26, despite rRMSE values being comparable to the healthy group. This discrepancy suggests that while the magnitude of errors may remain consistent, the temporal alignment between predicted and actual signals was poorer in injured subjects, likely due to the increased variability in their movement patterns.

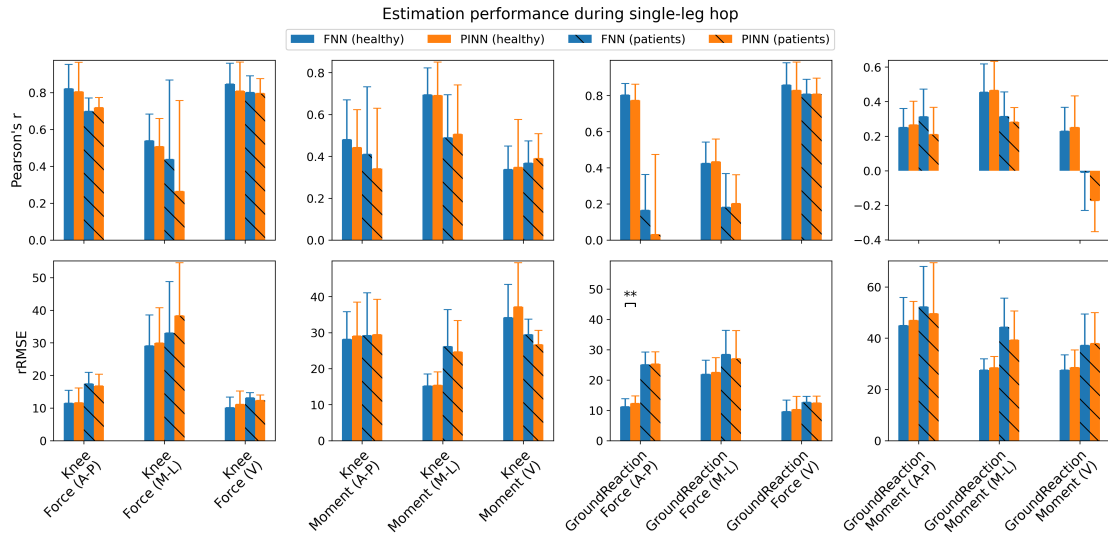


Figure 10. Comparison of Pearson's r correlation and rRMSE values of knee and ground reaction kinetic estimation during walking, between FNN and PINN in healthy and injured cohort. Kinetics include force components and moment around components (A-P = anterior-posterior, M-L=medial-lateral, V=vertical). Data are shown as mean + SD. Statistically significant differences are indicated: $p < 0.01$ (**).

3.3 Target knee kinetics within each cohort

Figure 11 presents the target KJFs across all individual trials during walking for both healthy and injured cohorts. In the healthy cohort, subjects showed consistent KJF patterns, particularly in the A-P and V directions. These directions exhibited smooth trajectories containing double peaks, characteristic the loading and puhs-off phases of walking. These components also showed relatively low inter-subject variability. In contrast, the M-L component showed greater variability across trials, with some trials even showing opposite trends. While the absolute magnitude of the M-L component was lower compared to the A-P and V components, its relative variability across trials was high. Since the data was regularized, this inconsistency in the M-L direction may have a disproportionate influence on model training, leading to biased error distribution. This pattern suggests a possible compensatory strategy aimed at minimizing lateral forces. Additionally, the A-P curves in the injured group appeared slightly flatter compared to those of healthy individuals, possibly reflecting reduced propulsion or altered gait mechanics.

In the injured cohort, similar overall trends were observed, showing stable trajectories in A-P and V directions and more inter-subject variability in the M-L direction. However, the injured cohort showed less variability overall, particularly in the M-L component. Additionally, the A-P curves in the injured cohort appeared slightly flatter compared to those of healthy subjects, possibly reflecting reduced propulsion or altered movement pattern.

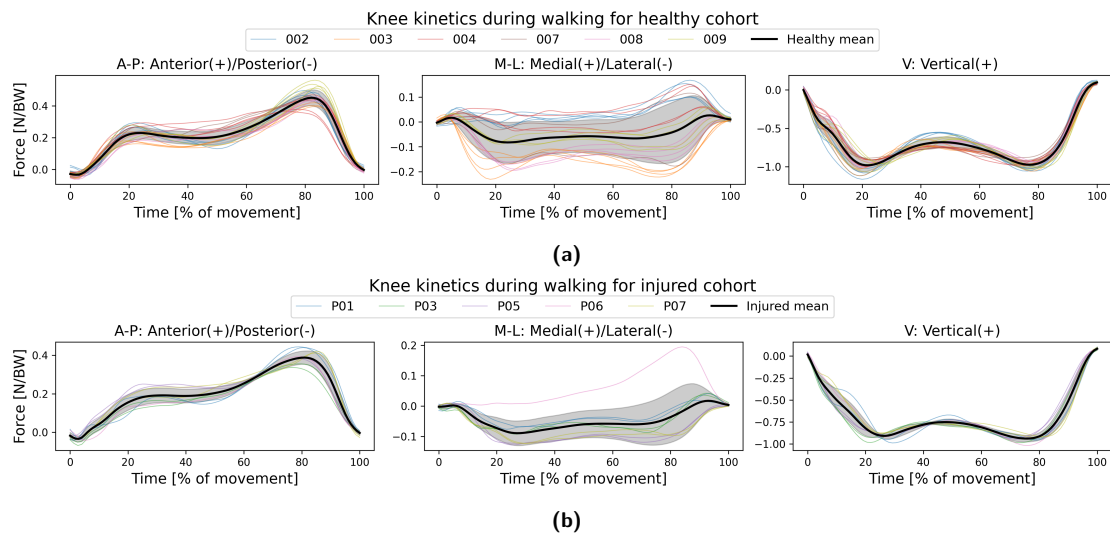


Figure 11. Individual KJF trajectories corresponding to subjects (subject number) and mean across subjects during walking for the healthy cohort (a) and injured cohort (b). Individual trajectories (colored lines), and cohort mean (black line) and SD (black shaded area) are shown.

Figure 12 presents the target KJFs across all individual trials during SLH for both cohorts. In the healthy cohort, consistent patterns were again observed across all directions. However, compared to walking, the shaded regions indicate increased inter-subject variability, particularly around peak force phases. The V component displayed a sharp impact peak early in the movement cycle at around 10–20%, with some subjects reaching forces near -2.0 N/BW. This reflects more dynamic and variable push-off or landing mechanics. In the A-P direction, several subjects exhibited force magnitudes close to or exceeding 1.0 N/BW, suggesting forceful push-off or landing strategies. Notably, some trials deviated substantially from the cohort mean, indicating potential outliers. These deviations, beyond variation in data, may affect model training by increasing prediction errors.

In contrast, the injured cohort exhibited more uniform force trajectories across all directions. The V and A-P components showed similar trajectories to those of the healthy cohort, but with notably reduced amplitudes. Less or no trials exceeded 1.0 N/BW in A-P or -2.0 N/BW in V direction. The reduced inter-subject variability and magnitude suggest a more constrained movement pattern during SLH.

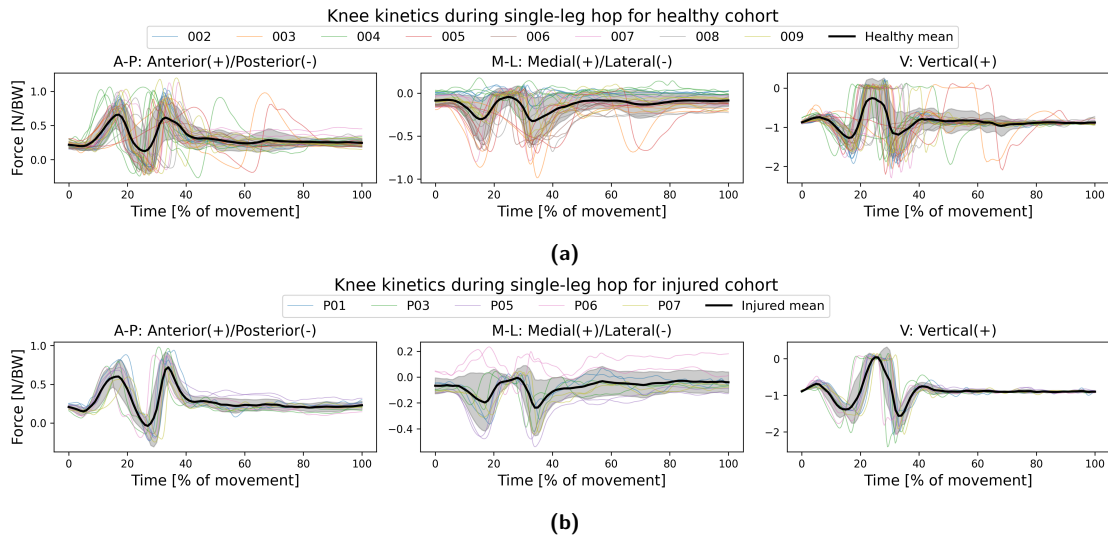


Figure 12. Individual KJF trajectories corresponding to subjects (subject number) and mean across subjects during SLH for the healthy cohort (a) and injured cohort (b). Individual mean (colored line) and SD (shaded area), as well as cohort mean (black line) are shown.

Additional results are provided in Appendix D. These include target KJMs within each cohort during walking (Figure D.4) and SLH (Figure D.5), as well as comparison of target knee joint and ground reaction kinetics across cohorts during walking and SLH (Figure D.6 and Figure D.7).

3.4 Effects of training data size

Figure 13 presents the performance of the PINN and baseline FNN models in estimating KJFs under varying training data size. The focus is on the relative effect of training data size on model accuracy.

The performance of estimating KJFs did not consistently improve with increasing training data size across components for either model. In the A-P direction, the PINN outperforms the FNN at 20% and 60% of training subjects included, but is slightly less accurate at 80% and 100%. In the V direction, both models perform similarly across most training sizes, with the PINN only slightly outperforming the FNN at 100% of training subjects. The most notable improvement is observed in the M-L direction, where performance improves substantially from 20% to 40% of the training subjects for both models.

For the KJMs, comparable observations were found to the KJFs. In the A-P direction, a notable improvement for both models is observed, similar to the M-L component of the KJFs. In the M-L direction, the PINN deteriorates when the percentage of total training subjects was increased from 80% to 100%, while the FNN improved between these percentages. Further, both models showed comparable performance across all percentages in the V direction.

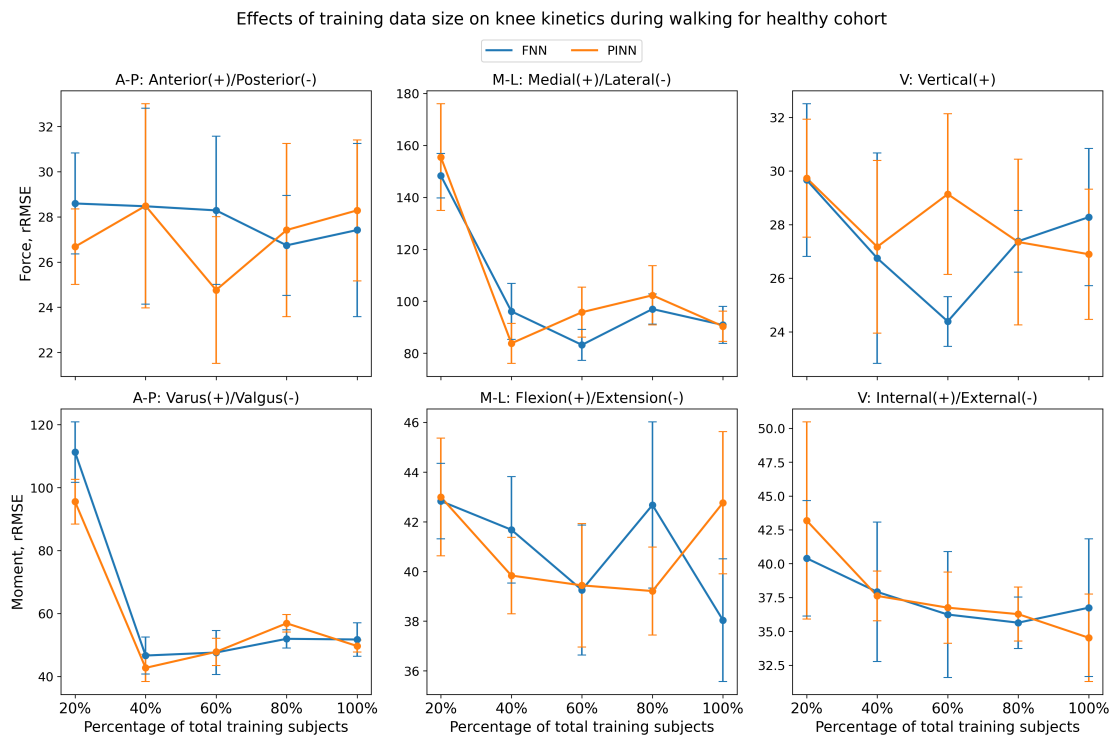


Figure 13. *rRMSE* values of KJFs estimation of the PINN and baseline FNN during walking for healthy cohort, under varying percentage of total training subjects. Data are shown as mean \pm SD.

3.5 Effects of physical loss weight

The effects on the performance of the PINN model in estimating KJFs under varying physical loss weighting is presented in Figure 14. As with training data size (see Section 3.4), the emphasis is on the relative performance changes rather than absolute improvements.

The performance of estimating KJFs appears to differ under varying physical loss weighting, but seems to be dependent on the component. In the A-P direction, the performance remained relatively consistent across different physical loss weights, with an improvement at a weight of 10. At this weight, the rRMSE dropped below the baseline FNN level. A similar trend was observed in the V direction, where performance stayed stable and consistently below the average rRMSE value corresponding to the baseline FNN. However, in M-L direction, performance deteriorates as physical loss weight increases. While lower weights (0.01 to 0.1) maintained rRMSE values near the average rRMSE of the baseline FNN, a clear increase in error was observed at higher weights, especially at 10 and 100.

For the KJMs, the performance appears to be dependent on the component as well. In the A-P direction, improvement was found at a physical weight of 1, while the model deteriorates at lower and higher weights. The opposite was observed in the M-L component, in which the highest error was found in the case of weight 1. In the V direction, the performance was observed to be stable across the weights, while being consistently below the average error associated with the FNN.

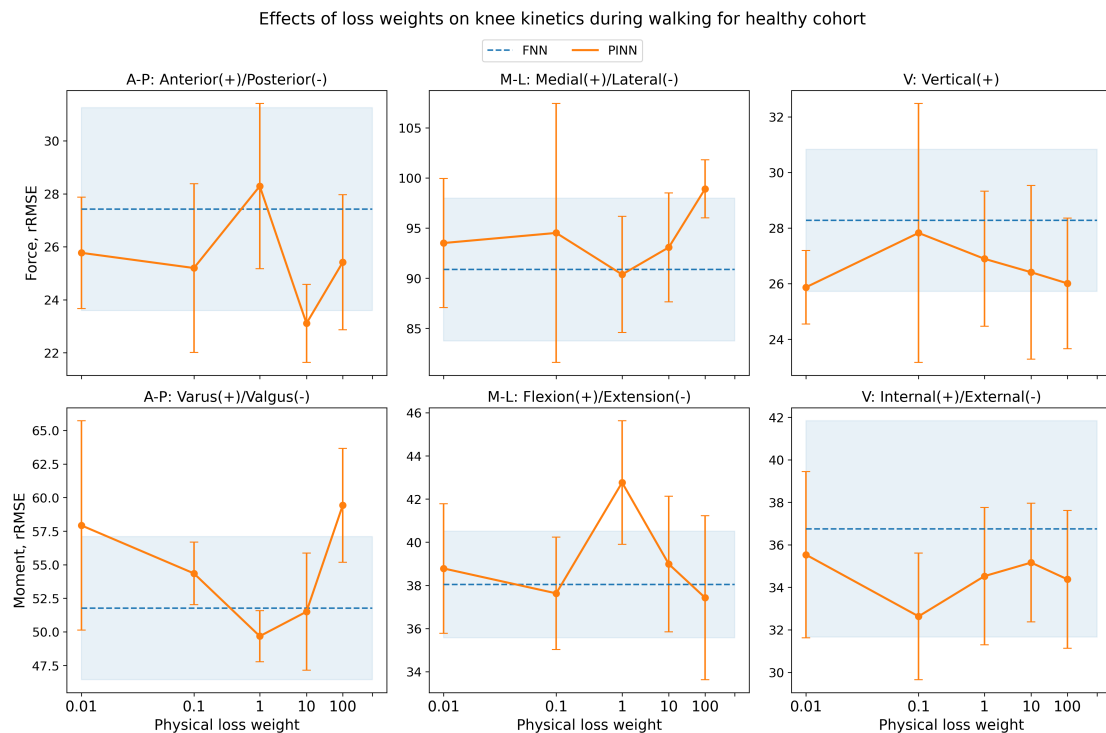


Figure 14. rRMSE values of KJFs estimation of the PINN during walking for healthy cohort, under varying physical loss weight. Additionally, the rRMSE value corresponding to the baseline FNN (dashed blue line) is shown as reference, which does not include the physical loss. Data are shown as mean \pm SD.

4 Discussion

This study evaluated the estimation performance of a PINN in estimating three-dimensional knee joint, as well as ground reaction, kinetics during walking and SLH in the context of ACLR rehabilitation. The findings reveal insights into the relative strengths and limitations of these model. To evaluate the effect of incorporating inverse dynamics during model training, the overall comparison is discussed in Section 4.1. In Section 4.2, the estimation performance of the PINN is evaluated across kinetic variables. Moreover, in Section 4.3, the influence of movement complexity and inter-subject variability is discussed. Further, limitations to this study are given in Section 4.5, and clinical implications can be found in Section 4.6. Additionally, recommendations on future research are described in Section 4.7.

4.1 Overall comparison

The comparison between PINN and FNN models revealed largely comparable overall performance across most kinetic variables. To the author's best knowledge, no study has yet beendone focusing on estimating knee joint and ground reaction kinetics using IMU-based segment kinematics and a PINN framework. Though, two similar studies were found, which proposed and evaluated a PINN framework for estimating joint angle and muscle forces based on surface electromyogram (sEMG) [50, 51]. Zhang et al [50] showed improved predictive accuracy of the PINN against several baseline machine learning methods in estimating knee joint angle and related muscle forces. Similarly, Ma et al. [51] found that the composite loss function, including rotational dynamics, was effective, as their PINN model achieved improved estimation performance against their baseline FNN model. Although not demonstrated in this study, previous studies do support the potential of physics-informed models in movement analysis to enhance both accuracy and biomechanical interpretation, particularly when estimating complex biomechanical outputs with limited or noisy data.

While both models performed well in dominant directions, the expected advantage of incorporating physical constraints for estimating components with lower magnitudes, such as the M-L forces, was limited and varied across conditions. Although such constraints were not directly incorporated into the neural network, Oh et al. [26] showed high estimation performance in these components as well using their hybrid model. In this study, the PINNs notably show significant improvements in estimating the KJM around A-P direction and the M-L component of the GRFs during walking. This highlights their ability to better capture underlying physical relationships in those directions. However, the FNN outperformed the PINN in estimating the GRM around the M-L axis during walking and the A-P component of the GRFs during SLH. These findings suggests that the data-driven models may offer advantages when movement deviate from standard patterns or physical assumptions are less reliable.

Regarding the physical assumptions, the rigid-body inverse dynamics embedded in the physical loss function fail to capture subject-specific anatomical variation, muscle force contribution, soft-tissue deformations, and other biomechanical nuances. Additionally, this assumption might not reflect altered movement patterns, potentially limiting the physical interpretation of especially ACLR patients [52]. Therefore, when applied to heterogeneous cohorts, the rigid-body assumption may fail to reflect true biomechanics, potentially limiting the accuracy of PINN estimations.

4.2 Evaluation on estimated kinetic variables

During both walking and SLH, the highest estimation performance was observed in the V and A-P components of the KJFs and GRFs. In particular, the V component of the GRFs appeared to be the most accurately estimated variable, with correlation coefficients frequently exceeding 0.90 and rRMSE values often below 15%, especially in the healthy cohort. Similarly, A-P forces, especially during SLH in the healthy cohort, showed strong performance, with some folds achieving rRMSE values below 10%. Similar observations for the GRFs were found by Leporace et al. [53] during walking, which reported correlation coefficients of 0.97 (A-P) and 0.98 (V) with error values of 1.8%BW (A-P) and 4.5%BW (V). Stetter et al. [25] as well found strong estimation performance in particular the V and A-P direction of KJFs, with correlation coefficients of 0.71 (A-P) and 0.87 (V) with rRMSE values of 20.8% (A-P) and 14.2% (V) during walking. The authors as well showed good estimation performance in these directions during push-off and landing phases of the SLH, reporting correlation coefficients ranging from 0.77 to 0.92 and rRMSE values between 15.4% and 25.1%.

Lower overall prediction performance was observed for the M-L force component. During walking, correlation coefficients ranged widely from 0.57 to 0.96, with rRMSE values between 9.89% and 35.14%. These findings align with previous studies reporting reduced estimation accuracy in the M-L direction. Leporace et al. [53] found lower correlations and higher errors in M-L components of the GRFs in compared to A-P and V directions, reporting a correlation of 0.80 and an error of 1.4%BW. Similarly, Stetter et al. [25] reported a correlation of 0.60 and an rRMSE value of 27.7% for the M-L component of KJFs during walking. The authors further found reductions during SLH, with correlations as low as 0.31 and 0.42 and rRMSE values up to 45.9%. The reduced accuracy in the M-L direction is often attributed to its lower magnitude, where small absolute errors lead to excessive large relative errors, strengthened by greater inter-subject variability [25, 53]. While these trends are consistent with previous findings, the absolute prediction performance observed in this study was lower. Nevertheless, some peak performances were observed in the M-L direction of GRFs during walking, with correlation coefficients exceeding 0.90 and rRMSE values below 10% in certain folds. This suggests that, under certain subject-specific movement patterns, challenging directions can be captured by the models.

Estimation of both KJMs and GRMs remained more challenging overall, showing lower estimation performance compared to force components. Similar trend were reported by Johnson et al. [54], who attributed the reduced correlations to potential misinterpretation of signal noise by the models. In contrast, Oh et al. [26] reported strong estimation performance across all components, with KJMs correlations ranging from 0.717 to 0.936, and GRMs from 0.841 and 0.987. In this study, relatively better performance was observed in specific cases. The V and M-L components of the KJMs showed promising results during SLH in the healthy cohort, with correlation coefficients up to 0.87 and rRMSE values as low as 9.39% for the M-L component. Similarly, the V component of GRMs performed relatively well during walking in the healthy cohort. These findings highlight underscore the difficulty of estimating joint and ground reaction moments from kinematic data alone, likely due to higher sensitivity to inter-subject variability and the complex dynamics involved in moment generation.

4.3 Movement complexity and inter-subject variability

Estimation performance was consistently better during walking compared to SLH, reflecting the lower complexity and greater regularity of walking. Walking involves symmetrical patterns with relatively consistent GRFs and joint kinetics across subjects. This was reflected in the stable KJF trajectories, particularly in the A-P and V directions, and lower inter-subject variability observed in both healthy and injured cohorts. In contrast, the SLH introduced greater complexity and subject specificity, especially in ACLR patients. This was reflected in increased variability across trials and the occurrence of outlier peaks. In part, these peaks may also resulted from challenges during data processing. Minor spatiotemporal misalignments, sensor positional errors, and time normalization could introduce inconsistencies in kinematic and kinetic estimations [23, 25, 33]. These factors, combined with the biomechanical complexity of SLH, likely contribute to the increased variability and presence of outliers.

The findings align with known influences on SLH variability, including limb dominance, neuromuscular compensation strategies, fatigue, and pain-related adaptations [8]. Gokeler et al. [8] reported altered neuromuscular control in ACLR patients during SLH, typically involving reduced knee joint loading on the injured limb. In this study, this trend was also observed through reduced KJFs in the injured cohort during SLH, despite the dynamic demands of the movement.

During walking, injured subjects exhibited lower peak forces than healthy subjects, which is consistent with findings of reduced peak knee flexion/extension moments and altered GRFs in ACLR [12–14]. Additionally, across both walking and SLH, the injured cohort showed less inter-subject variability compared to the healthy cohort. This may indicate reduced movement patterns or intentional compensation strategies, supporting findings by Rohman et al. and Moya-Angeler et al. [15, 16]. These studies reported reduced GRFs in V direction and GRMs in sagittal plane during SLH in injured limbs.

In addition, these findings highlight the importance of considering inter-subject variability when evaluating robustness and generalizability of prediction models [44, 45]. As emphasized by Stetter et al. [49], generalizing across different movements and cohorts is particularly challenging for components with low magnitudes, such as those in the M-L direction. These components are more sensitive to noise and subject-specific differences. This study underscores the need for models that can capture movement and subject-specific variability.

4.4 Training data size and physical loss weighting

The PINN did not consistently outperform across all components of the KJFs and KJMs, particularly at lower amount of training data. This is not in accordance with previous studies on PINNs, which emphasize the performance in scenarios with limited amount of data [30, 50]. For instance, Karniadakis et al. [30] highlighted the accuracy of PINNs in learning from limited data by embedding physical constraints to compensate for sparse datasets. Similarly and more relevant to this study, Zhang et al. [50] reported lower normalized RMSE (nRMSE) values for a PINN-based framework compared to baseline data-driven models, suggesting clear advantages when data availability is limited.

In addition to the performance on limited data, both PINN and FNN models did not show consistent improvement in estimation accuracy with increasing training data size. This is also inconsistent with the findings of Zhang et al. [50], who showed a clear decrease in nRMSE values with an increasing number of training data for all tested models. This discrepancy may be caused by the heterogeneity of the training data. As more subjects are added to increase the data size, inter-subject variability may introduce additional complexity. This could counteract the benefits of increased data size. These findings underscore the importance of the quantity as well as the quality and consistency of training data when developing data-driven and physics-informed models in the context of ACLR rehabilitation.

Varying the physical weighting within the composite loss function of the PINN framework did not result in consistent improvements in estimation performance across all components of the KJFs and KJMs. Although estimation accuracy was influenced with varying weight, this effect was direction-dependent. These findings are partially in line with previous studies that have examined the sensitivity of PINN performance to the relative contribution of physics-informed against data-driven term in the composite loss function [55, 56]. Wang et al. [55] and Cao et al. [56] showed that the accuracy of PINNs can be significantly influenced by irregular loss weighting. The authors emphasized the importance of dynamically balancing the influence of each component during training. These findings underscore that model performance in PINNs is highly sensitive to the choice of loss function weighting. As such, the use of a static or empirically tuned weighting scheme may not generalize well across components.

4.5 Limitations

This study has several limitations that should be considered when interpreting the results and assessing their applicability. First, assumptions were made in the design and implementation of the PINN framework in this study. The model structure, architecture, and regularization strategies may not completely align with the original principles of physics-informed learning [29, 30]. Alternative model designs or loss function formulations may enhance estimation accuracy and robustness [50, 51].

Further, the dataset was limited in size. A smaller sample size may restrict the model's ability to generalize across broader cohorts and may increase the risk of overfitting. This is particularly important in the context of ML approaches, where larger dataset often improve robustness and predictive accuracy [25].

In addition, each patient was measured only once at an unknown and potentially varying phase of their rehabilitation. Although the subject characteristics was reported, it did not fully capture rehabilitation status. Patients at different phases may exhibit different movement patterns and compensation strategies, affecting both kinetics and model performance [7, 8]. Other inter-subject differences, such as age, baseline activity level, and injury history were not accounted for and could have influenced variability in both biomechanics and model estimation accuracy [57]. Furthermore, all exercises were performed in a constrained laboratory setting. In particular, the fixed positioning of the force plates required subjects to adjust their movements to ensure accurate foot placement. This constraint could have introduced artifacts in both walking and SLH mechanics, potentially limiting the ecological validity of the findings [21]. Additionally, only two performance tests were evaluated in this study, including walking and SLH. While both are commonly used in clinical evaluations, ACLR rehabilitation involves a broader test battery, which are critical for RTS assessment [7, 9, 10, 58].

Lastly, although figures illustrating kinematic variable importance are included in Appendix E, they were not analyzed within the main text. These results offer potential insights into sensor contributions across conditions. A more detailed investigation is needed to determine whether certain sensor consistently influence estimation performance and whether sensor configurations could be optimized for on-field measurements [27, 33].

4.6 Clinical implications

This study shows the potential of combining IMUs with ML approaches to estimate knee joint kinetics during movements relevant in ACLR rehabilitation. Unlike earlier studies that primarily focused on walking and running in healthy cohorts [25–28], this work extends kinetic estimation to functional tests relevant for RTS decision-making [8, 12].

The use of IMUs and neural networks presents a promising solution for translating joint kinetics beyond laboratory setting. Such tools could offer clinicians objective and quantitative insights into joint loading during performance tests, supporting more individualized and data-driven RTS decision [8, 12]. This is particularly valuable given the limitations of current assessments and the importance of addressing movement quality and asymmetries after ACLR [7].

However, the current findings are constrained by the laboratory setting. Movement execution was influenced by force plate positioning, potentially altering natural movement patterns. Additionally, only two functional tests were evaluated, while ACLR rehabilitation usually involves more movement assessments. The single time point per subject in lab-dependent environment further limits the generalizability of the model across different phases of ACLR rehabilitation and real-world settings.

4.7 Future research

Several aspects for future research are recommended to address the current limitations and enhance the applicability of estimating knee kinetics using IMUs during ACLR rehabilitation.

Regarding the designed PINN framework, there is potential to adjust the physical loss function for enhancing model accuracy and interpretation. The current physical loss containing segment-based inverse dynamics could be extended to include musculoskeletal dynamics, enabling estimation of both joint and muscle forces. Integration of software like OpenSim [59] and approaches such as those from Zhang et al. [50] and Ma et al. [51] could provide more interpretable and biomechanical valid outputs.

Another recommendation focuses on the loss balancing within the PINN framework. The relative weighting between data-driven and physics-informed loss components affects model performance [55, 56]. Future research should could explore a balanced composite loss function to optimize performance while preserving biomechanical validity [56, 60, 61].

Model structure or architecture is another aspect for potential improvement. While a FNN was used in this study, alternative architectures may better capture the temporal dynamics of movement. Recurrent neural networks (RNNs), including LSTM models, are well-suited for time series data and could enhance the prediction of joint kinetics during cyclic and non-cyclic tasks [62, 63]. Ensemble learning strategies may also improve robustness and generalization across subjects and movement tasks [27].

In addition, a broader and more diverse set of data is essential. Future studies should include a larger cohort of participants, capture data across different phases of rehabilitation, and incorporate on-field measurements. Lab-based assessments using OMC system remain important, particular for validation purposes. Though, longitudinal, on-field measurements are essential for supporting RTS decision making [21]. Additionally, expanding the range of movements beyond walking and SLH is necessary. Exercises such as single-leg lateral hops, vertical drop jumps or squats offer additional insights during rehabilitation [6, 8].

In the longer term, once robust and accurate estimation of knee joint kinetics have been achieved, future research could expand toward asymmetry analysis. Previous studies have reported significant differences in knee kinetics between the injured and contralateral limbs [8, 15, 16]. Assessing limb asymmetry is of clinical importance in ACLR rehabilitation, as it provides insights into recovery, compensatory strategies, and reinjury risk. However, this analysis requires high estimation accuracy for each limb independently. Therefore, developing robust models across diverse cohorts is necessary before extending the current approach to subject-specific, inter-limb comparison.

5 Conclusion

This study showed the feasibility of estimating knee joint kinetics from IMUs using a physics-informed approach, specifically during walking and SLH in the context of ACLR rehabilitation. A data processing pipeline was developed to spatiotemporally align and generalize existing IMC and OMC data. Kinematic data was translated and rotated to reflect anatomical coordinate frames, enabling compatibility with inverse dynamics analyses and meaningful inputs to neural network models.

The data processing pipeline allowed for the extraction of segment kinematics in a way that mimicked the Xsens MVN biomechanical model, while simultaneously enabling application of three-dimensional inverse dynamics. These kinematic variables were then implemented into as input to an adaptable neural network framework, which incorporated a physical loss function. The physical loss, derived from three-dimensional translational and rotational dynamics, utilized the input kinematics, estimated output kinetics, and pre-defined scaling ratios. The training process employed a composite loss function that satisfied both data-driven and physical constraints, which guided the model's learning process toward biomechanical interpretable estimations.

Although the PINN framework incorporated biomechanical constraints into the training process, it did not lead to improved estimation performance over the baseline FNN. Both models showed predictive challenges, which were particularly observed for kinetic components in the M-L direction. This is likely due to their lower magnitudes and greater sensitivity to noise, consistent with prior literature. Moreover, compared to other studies that employed estimation models, the overall performance of both networks was relatively modest. These findings emphasize that incorporating physical constraints does not lead to improved predictive accuracy, particularly under conditions of limited data or variability in subject movement patterns.

Despite these findings, this study provides an important basis toward physics-informed learning approaches in ACLR rehabilitation. The approach enabled biomechanical interpretation of kinetic estimates while highlighting the important methodological challenges, including model architecture, loss balancing, and data availability.

Together, these contributions answered the research question by showing that three-dimensional inverse dynamics can be successfully incorporated into a PINN to estimate knee kinetics from IMU data. However, this incorporation did not improve prediction accuracy over a baseline model under the current conditions, disproving the initial hypothesis.

Further development should focus on enhancing model robustness through improvements on the framework, adaptive loss balancing, and broader datasets. When sufficient estimation accuracy is achieved, these models may be extended to clinically relevant applications, such as subject-specific assessments of limb asymmetry. Such improvements have the potential to contribute to more objective and individualized RTS decision-making and ultimately help reduce the risk of reinjury following ACLR.

References

- [1] J. Evans, A. Mabrouk, and J. I. Nielson, "Anterior Cruciate Ligament Knee Injury," *StatPearls*, Nov. 2023.
- [2] S. M. Jenkins *et al.*, "Rehabilitation After Anterior Cruciate Ligament Injury: Review of Current Literature and Recommendations," *Current Reviews in Musculoskeletal Medicine*, vol. 15, no. 3, p. 170, Jun. 2022, ISSN: 19359748. DOI: 10.1007/S12178-022-09752-9.
- [3] E. N. Marieb and K. Hoehn, "Joints," in *Human Anatomy & Physiology*, 11th, Pearson Education, 2019, ch. 8, pp. 302–304, ISBN: 978-1-292-26085-3.
- [4] P. Shom, A. R. Varma, and R. Prasad, "The Anterior Cruciate Ligament: Principles of Treatment," *Cureus*, vol. 15, no. 6, Jun. 2023. DOI: 10.7759/CUREUS.40269.
- [5] R. Hoogeslag, "Anterior Cruciate Ligament Repair: The Quest Continues," Ph.D. dissertation, University of Twente, 2022, ISBN: 978-90-365-5457-2. DOI: <https://doi.org/10.3990/1.9789036554572>.
- [6] A. Gokeler, W. Welling, S. Zaffagnini, R. Seil, and D. Padua, "Development of a test battery to enhance safe return to sports after anterior cruciate ligament reconstruction," *Knee Surgery, Sports Traumatology, Arthroscopy*, vol. 25, no. 1, pp. 192–199, Jan. 2017, ISSN: 14337347. DOI: 10.1007/S00167-016-4246-3/FIGURES/3.
- [7] A. Gokeler, B. Dingenen, and T. E. Hewett, "Rehabilitation and Return to Sport Testing After Anterior Cruciate Ligament Reconstruction: Where Are We in 2022?" *Arthroscopy, Sports Medicine, and Rehabilitation*, vol. 4, no. 1, e77–e82, Jan. 2022, ISSN: 2666-061X. DOI: 10.1016/J.ASMR.2021.10.025.
- [8] A. Gokeler, W. Welling, A. Benjaminse, K. Lemmink, R. Seil, and S. Zaffagnini, "A critical analysis of limb symmetry indices of hop tests in athletes after anterior cruciate ligament reconstruction: A case control study," *Orthopaedics and Traumatology: Surgery and Research*, vol. 103, no. 6, pp. 947–951, Oct. 2017, ISSN: 18770568. DOI: 10.1016/j.otsr.2017.02.015.
- [9] C. Roe, C. Jacobs, J. Hoch, D. L. Johnson, and B. Noehren, "Test Batteries After Primary Anterior Cruciate Ligament Reconstruction: A Systematic Review," *Sports Health*, vol. 14, no. 2, p. 205, Mar. 2022, ISSN: 19410921. DOI: 10.1177/19417381211009473.
- [10] "ACL Melbourne ACL Rehabilitation Guide 2.0,"
- [11] S. L. Di Stasi, D. Logerstedt, E. S. Gardinier, and L. Snyder-Mackler, "Gait Patterns Differ Between ACL-Reconstructed Athletes Who Pass Return-to-Sport Criteria and Those Who Fail," *The American journal of sports medicine*, vol. 41, no. 6, p. 1310, Jun. 2013, ISSN: 15523365. DOI: 10.1177/0363546513482718.
- [12] L. V. Slater, J. M. Hart, A. R. Kelly, and C. M. Kuenze, "Progressive Changes in Walking Kinematics and Kinetics After Anterior Cruciate Ligament Injury and Reconstruction: A Review and Meta-Analysis," *Journal of Athletic Training*, vol. 52, no. 9, p. 847, Sep. 2017, ISSN: 1938162X. DOI: 10.4085/1062-6050-52.6.06.
- [13] R. K. Varma, L. D. Duffell, D. Nathwani, and A. H. McGregor, "Knee moments of anterior cruciate ligament reconstructed and control participants during normal and inclined walking," *BMJ Open*, vol. 4, no. 6, p. 4753, 2014, ISSN: 20446055. DOI: 10.1136/BMJOPEN-2013-004753.
- [14] M. E. Zabala, J. Favre, S. F. Scanlan, J. Donahue, and T. P. Andriacchi, "Three-Dimensional Knee Moments of ACL Reconstructed and Control Subjects during Gait, Stair Ascent, and Stair Descent," *Journal of biomechanics*, vol. 46, no. 3, p. 515, Feb. 2013, ISSN: 00219290. DOI: 10.1016/J.JBIOMECH.2012.10.010.
- [15] E. Rohman, J. T. Steubs, and M. Tompkins, "Changes in Involved and Uninvolved Limb Function During Rehabilitation After Anterior Cruciate Ligament Reconstruction: Implications for Limb Symmetry Index Measures," *American Journal of Sports Medicine*, vol. 43, no. 6, pp. 1391–1398, Jun. 2015, ISSN: 15523365. DOI: 10.1177/0363546515576127/ASSET/IMAGES/LARGE/10.1177/0363546515576127-FIG3.JPEG.
- [16] J. Moya-Angeler, J. Vaquero, and F. Forriol, "Evaluation of lower limb kinetics during gait, sprint and hop tests before and after anterior cruciate ligament reconstruction," *Journal of Orthopaedics and Traumatology : Official Journal of the Italian Society of Orthopaedics and Traumatology*, vol. 18, no. 2, p. 177, Jun. 2017, ISSN: 15909999. DOI: 10.1007/S10195-017-0456-9.
- [17] S. Di Paolo *et al.*, "Rehabilitation and Return to Sport Assessment after Anterior Cruciate Ligament Injury: Quantifying Joint Kinematics during Complex High-Speed Tasks through Wear-

- able Sensors," *Sensors (Basel, Switzerland)*, vol. 21, no. 7, Apr. 2021, ISSN: 14248220. DOI: 10.3390/S21072331.
- [18] A. V. Dowling, J. Favre, and T. P. Andriacchi, "Inertial Sensor-Based Feedback Can Reduce Key Risk Metrics for Anterior Cruciate Ligament Injury During Jump Landings," *The American Journal of Sports Medicine*, 2012. DOI: 10.1177/0363546512437529.
- [19] M. P. Kadaba, H. K. Ramakrishnan, and M. E. Wootten, "Measurement of lower extremity kinematics during level walking," *Journal of Orthopaedic Research*, vol. 8, no. 3, pp. 383–392, 1990, ISSN: 1554527X. DOI: 10.1002/JOR.1100080310.
- [20] D. A. Winter, "Biomechanics and Motor Control of Human Movement: Fourth Edition," *Biomechanics and Motor Control of Human Movement: Fourth Edition*, pp. 1–370, Sep. 2009. DOI: 10.1002/9780470549148.
- [21] E. M. Nijmeijer, P. Heuvelmans, R. Bolt, A. Gokeler, E. Otten, and A. Benjaminse, "Concurrent validation of the Xsens IMU system of lower-body kinematics in jump-landing and change-of-direction tasks," *Journal of Biomechanics*, vol. 154, p. 111 637, Jun. 2023, ISSN: 0021-9290. DOI: 10.1016/J.JBIOMECH.2023.111637.
- [22] E. Ceseracciu, Z. Sawacha, and C. Cobelli, "Comparison of Markerless and Marker-Based Motion Capture Technologies through Simultaneous Data Collection during Gait: Proof of Concept," *PLOS ONE*, vol. 9, no. 3, e87640, Mar. 2014, ISSN: 1932-6203. DOI: 10.1371/JOURNAL.PONE.0087640.
- [23] D. Roetenberg, H. Luinge, and P. Slycke, "Xsens MVN: Full 6DOF Human Motion Tracking Using Miniature Inertial Sensors," vol. 8, 2009.
- [24] S. Krishnakumar, B. J. F. van Beijnum, C. T. Baten, P. H. Veltink, and J. H. Buurke, "Estimation of Kinetics Using IMUs to Monitor and Aid in Clinical Decision-Making during ACL Rehabilitation: A Systematic Review," *Sensors*, vol. 24, no. 7, p. 2163, Apr. 2024, ISSN: 14248220. DOI: 10.3390/S24072163/S1.
- [25] B. J. Stetter, S. Ringhof, F. C. Krafft, S. Sell, and T. Stein, "Estimation of Knee Joint Forces in Sport Movements Using Wearable Sensors and Machine Learning," *Sensors 2019, Vol. 19, Page 3690*, vol. 19, no. 17, p. 3690, Aug. 2019, ISSN: 1424-8220. DOI: 10.3390/S19173690.
- [26] S. E. Oh, A. Choi, and J. H. Mun, "Prediction of ground reaction forces during gait based on kinematics and a neural network model," *Journal of Biomechanics*, vol. 46, no. 14, pp. 2372–2380, Sep. 2013, ISSN: 0021-9290. DOI: 10.1016/J.JBIOMECH.2013.07.036.
- [27] B. L. Scheltinga, J. N. Kok, J. H. Buurke, and J. Reenalda, "Estimating 3D ground reaction forces in running using three inertial measurement units," *Frontiers in Sports and Active Living*, vol. 5, p. 1 176 466, May 2023, ISSN: 26249367. DOI: 10.3389/FSPOR.2023.1176466/BIBTEX.
- [28] R. D. Gurchiek, N. Donahue, N. M. Fiorentino, and R. S. McGinnis, "Wearables-Only Analysis of Muscle and Joint Mechanics: An EMG-Driven Approach," *IEEE Transactions on Biomedical Engineering*, vol. 69, no. 2, pp. 580–589, Feb. 2022, ISSN: 15582531. DOI: 10.1109/TBME.2021.3102009.
- [29] M. Raissi, P. Perdikaris, and G. E. Karniadakis, "Physics-informed neural networks: A deep learning framework for solving forward and inverse problems involving nonlinear partial differential equations," *Journal of Computational Physics*, vol. 378, pp. 686–707, Feb. 2019, ISSN: 0021-9991. DOI: 10.1016/J.JCP.2018.10.045.
- [30] G. E. Karniadakis, I. G. Kevrekidis, L. Lu, P. Perdikaris, S. Wang, and L. Yang, "Physics-informed machine learning," *Nature Reviews Physics 2021 3:6*, vol. 3, no. 6, pp. 422–440, May 2021, ISSN: 2522-5820. DOI: 10.1038/s42254-021-00314-5.
- [31] L. Sun, H. Gao, S. Pan, and J. X. Wang, "Surrogate modeling for fluid flows based on physics-constrained deep learning without simulation data," *Computer Methods in Applied Mechanics and Engineering*, vol. 361, p. 112 732, Apr. 2020, ISSN: 0045-7825. DOI: 10.1016/J.CMA.2019.112732.
- [32] V. Yogesh *et al.*, "UWB distance estimation errors in (non-)line of sight situations within the context of 3D analysis of human movement," *Engineering Research Express*, vol. 6, no. 4, p. 045 303, Oct. 2024, ISSN: 2631-8695. DOI: 10.1088/2631-8695/AD7E7E.
- [33] F. J. Wouda *et al.*, "Estimation of vertical ground reaction forces and sagittal knee kinematics during running using three inertial sensors," *Frontiers in Physiology*, vol. 9, no. MAR, p. 328 581, Mar. 2018, ISSN: 1664042X. DOI: 10.3389/FPHYS.2018.00218/BIBTEX.
- [34] J. H. Challis, "Quaternions as a solution to determining the angular kinematics of human movement," *BMC Biomedical Engineering*, vol. 2, no. 1, p. 5, Dec. 2020. DOI: 10.1186/S42490-020-00039-Z.

- [35] W. H. de Vries, H. E. Veeger, C. T. Baten, and F. C. van der Helm, "Magnetic distortion in motion labs, implications for validating inertial magnetic sensors," *Gait & Posture*, vol. 29, no. 4, pp. 535–541, Jun. 2009, ISSN: 0966-6362. DOI: 10.1016/J.GAITPOST.2008.12.004.
- [36] A. Longo, T. Haid, R. Meulenbroek, and P. Federolf, "Biomechanics in posture space: Properties and relevance of principal accelerations for characterizing movement control," *Journal of Biomechanics*, vol. 82, pp. 397–403, Jan. 2019, ISSN: 0021-9290. DOI: 10.1016/J.JBIOMECH.2018.11.031.
- [37] R. Taylor, "Interpretation of the Correlation Coefficient: A Basic Review," *Journal of Diagnostic Medical Sonography*, vol. 6, no. 1, pp. 35–39, 1990, ISSN: 15525430. DOI: 10.1177/875647939000600106.
- [38] L. Ren, R. K. Jones, and D. Howard, "Whole body inverse dynamics over a complete gait cycle based only on measured kinematics," *Journal of Biomechanics*, vol. 41, no. 12, pp. 2750–2759, Aug. 2008, ISSN: 0021-9290. DOI: 10.1016/J.JBIOMECH.2008.06.001.
- [39] P. De Leva, "Adjustments to Zatsiorsky-Seluyanov's segment inertia parameters," *Journal of Biomechanics*, vol. 29, no. 9, pp. 1223–1230, Sep. 1996, ISSN: 0021-9290. DOI: 10.1016/0021-9290(95)00178-6.
- [40] J. W. Wannop, J. T. Worobets, and D. J. Stefanyshyn, "Normalization of Ground Reaction Forces, Joint Moments, and Free Moments in Human Locomotion," *Journal of Applied Biomechanics*, vol. 28, no. 6, pp. 665–676, Dec. 2012, ISSN: 1065-8483. DOI: 10.1123/JAB.28.6.665.
- [41] B. Van Hooren, S. M. Hirsch, and K. Meijer, "A comparison of five methods to normalize joint moments during running," *Gait & Posture*, vol. 105, pp. 81–86, Sep. 2023, ISSN: 0966-6362. DOI: 10.1016/J.GAITPOST.2023.07.278.
- [42] A. S. Bley, J. C. F. Correa, A. C. D. Reis, N. D. D. A. Rabelo, P. H. Marchetti, and P. R. G. Lucareli, "Propulsion Phase of the Single Leg Triple Hop Test in Women with Patellofemoral Pain Syndrome: A Biomechanical Study," *PLOS ONE*, vol. 9, no. 5, e97606, May 2014, ISSN: 1932-6203. DOI: 10.1371/JOURNAL.PONE.0097606.
- [43] A. Paszke *et al.*, "PyTorch: An Imperative Style, High-Performance Deep Learning Library," *Advances in Neural Information Processing Systems*, vol. 32, Dec. 2019, ISSN: 10495258.
- [44] Z. Altai, I. Boukhenoufa, X. Zhai, A. Phillips, J. Moran, and B. X. Liew, "Performance of multiple neural networks in predicting lower limb joint moments using wearable sensors," *Frontiers in Bioengineering and Biotechnology*, vol. 11, p. 1215770, Jul. 2023, ISSN: 22964185. DOI: 10.3389/FBIOE.2023.1215770/BIBTEX.
- [45] L. Xiang, A. Wang, Y. Gu, L. Zhao, V. Shim, and J. Fernandez, "Recent Machine Learning Progress in Lower Limb Running Biomechanics With Wearable Technology: A Systematic Review," *Frontiers in Neurorobotics*, vol. 16, p. 913052, Jun. 2022, ISSN: 16625218. DOI: 10.3389/FNBOT.2022.913052/BIBTEX.
- [46] E. Halilaj, A. Rajagopal, M. Fiterau, J. L. Hicks, T. J. Hastie, and S. L. Delp, "Machine learning in human movement biomechanics: Best practices, common pitfalls, and new opportunities," *Journal of Biomechanics*, vol. 81, pp. 1–11, Nov. 2018, ISSN: 0021-9290. DOI: 10.1016/J.JBIOMECH.2018.09.009.
- [47] I. T. Jolliffe and J. Cadima, "Principal component analysis: a review and recent developments," *Philosophical Transactions of the Royal Society A: Mathematical, Physical and Engineering Sciences*, vol. 374, no. 2065, Apr. 2016, ISSN: 1364503X. DOI: 10.1098/RSTA.2015.0202.
- [48] T. Akiba, S. Sano, T. Yanase, T. Ohta, and M. Koyama, "Optuna: A Next-generation Hyperparameter Optimization Framework," *Proceedings of the ACM SIGKDD International Conference on Knowledge Discovery and Data Mining*, pp. 2623–2631, Jul. 2019. DOI: 10.1145/3292500.3330701.
- [49] B. J. Stetter, F. C. Krafft, S. Ringhof, T. Stein, and S. Sell, "A Machine Learning and Wearable Sensor Based Approach to Estimate External Knee Flexion and Adduction Moments During Various Locomotion Tasks," *Frontiers in Bioengineering and Biotechnology*, vol. 8, no. 9, p. 508120, Jan. 2020, ISSN: 22964185. DOI: 10.3389/FBIOE.2020.00009/BIBTEX.
- [50] J. Zhang *et al.*, "Physics-Informed Deep Learning for Musculoskeletal Modeling: Predicting Muscle Forces and Joint Kinematics From Surface EMG," *IEEE Transactions on Neural Systems and Rehabilitation Engineering*, vol. 31, pp. 484–493, 2023, ISSN: 15580210. DOI: 10.1109/TNSRE.2022.3226860.
- [51] S. Ma, J. Zhang, C. Shi, P. Di, I. D. Robertson, and Z. Q. Zhang, "Physics-Informed Deep Learning for Muscle Force Prediction with Unlabeled sEMG Signals," *IEEE Transactions on*

- Neural Systems and Rehabilitation Engineering*, vol. 32, pp. 1246–1256, 2024, ISSN: 15580210. DOI: 10.1109/TNSRE.2024.3375320.
- [52] M. J. Schroeder, C. Krishnan, and Y. Y. Dhaher, “The influence of task complexity on knee joint kinetics following ACL reconstruction,” *Clinical Biomechanics*, vol. 30, no. 8, pp. 852–859, Oct. 2015, ISSN: 0268-0033. DOI: 10.1016/J.CLINBIOMECH.2015.06.003.
- [53] G. Leporace, L. A. Batista, and J. Nadal, “Prediction of 3D ground reaction forces during gait based on accelerometer data,” *Research on Biomedical Engineering*, vol. 34, no. 3, pp. 211–216, Sep. 2018, ISSN: 2446-4732. DOI: 10.1590/2446-4740.06817.
- [54] W. R. Johnson, A. Mian, M. A. Robinson, J. Verheul, D. G. Lloyd, and J. A. Alderson, “Multidimensional Ground Reaction Forces and Moments from Wearable Sensor Accelerations via Deep Learning,” *IEEE Transactions on Biomedical Engineering*, vol. 68, no. 1, pp. 289–297, Jan. 2021, ISSN: 15582531. DOI: 10.1109/TBME.2020.3006158.
- [55] S. Wang, Y. Teng, and P. Perdikaris, “Understanding and mitigating gradient flow pathologies in physics-informed neural networks,” *SIAM Journal on Scientific Computing*, vol. 43, no. 5, pp. 3055–3081, 2021, ISSN: 10957197. DOI: 10.1137/20M1318043/SUPPL{_}_FILE/SUPPLEMENTARY.PDF.
- [56] F. Cao, X. Guo, X. Dong, and D. Yuan, “wbPINN: Weight balanced physics-informed neural networks for multi-objective learning,” *Applied Soft Computing*, vol. 170, p. 112 632, Feb. 2025, ISSN: 1568-4946. DOI: 10.1016/J.ASOC.2024.112632.
- [57] B. Dingenen and A. Gokeler, “Optimization of the Return-to-Sport Paradigm After Anterior Cruciate Ligament Reconstruction: A Critical Step Back to Move Forward,” *Sports Medicine* 2017 47:8, vol. 47, no. 8, pp. 1487–1500, Jan. 2017, ISSN: 1179-2035. DOI: 10.1007/S40279-017-0674-6.
- [58] A. Gustavsson *et al.*, “A test battery for evaluating hop performance in patients with an ACL injury and patients who have undergone ACL reconstruction,” *Knee Surgery, Sports Traumatology, Arthroscopy*, vol. 14, no. 8, pp. 778–788, Aug. 2006, ISSN: 09422056. DOI: 10.1007/S00167-006-0045-6/TABLES/6.
- [59] A. Seth *et al.*, “OpenSim: Simulating musculoskeletal dynamics and neuromuscular control to study human and animal movement,” *PLOS Computational Biology*, vol. 14, no. 7, e1006223, Jul. 2018, ISSN: 1553-7358. DOI: 10.1371/JOURNAL.PCBI.1006223.
- [60] Z. Chen, V. Badrinarayanan, C. Y. Lee, and A. Rabinovich, “GradNorm: Gradient Normalization for Adaptive Loss Balancing in Deep Multitask Networks,” *35th International Conference on Machine Learning, ICML 2018*, vol. 2, pp. 1240–1251, Nov. 2017.
- [61] Z. Xiang, W. Peng, X. Liu, and W. Yao, “Self-adaptive loss balanced Physics-informed neural networks,” *Neurocomputing*, vol. 496, pp. 11–34, Jul. 2022, ISSN: 0925-2312. DOI: 10.1016/J.NEUCOM.2022.05.015.
- [62] D. Lalonde-Larocque, N. Mezghani, N. J. Bureau, R. Aissaoui, and N. Hagemester, “Triaxial knee joint kinematics estimation from inertial measurement units using LSTM neural networks,” *Multidisciplinary Biomechanics Journal*, vol. 49th congress, no. Biomechanics and artificial... Jan. 2025, ISSN: 3076-1158. DOI: 10.46298/MBJ.14518.
- [63] R. Sugai *et al.*, “LSTM Network-Based Estimation of Ground Reaction Forces during Walking in Stroke Patients Using Markerless Motion Capture System,” *IEEE Transactions on Medical Robotics and Bionics*, vol. 5, no. 4, pp. 1016–1024, Nov. 2023, ISSN: 25763202. DOI: 10.1109/TMRB.2023.3310196.

Appendix

A Declarations

Images

"During the preparation of this work, visual materials were sourced from VectorStock and BioRender to enhance the clarity and communication of key concepts. These resources were used solely for non-commercial, academic purposes within the context of this master's thesis. No licenses were purchased for these materials. The author acknowledges the copyright of the original creators and has made efforts to credit these sources appropriately. The final use and integration of all images are the sole responsibility of the author."

AI use

"During the preparation of this work, I used ChatGPT (OpenAI) and Copilot (Microsoft) to support refinement of grammar and wording, assistance with writing and debugging MATLAB and Python code, and support with LaTeX formatting. After using this tool, the author thoroughly reviewed and edited the content as needed, taking full responsibility for the final outcome."

B Data processing pipeline

A detailed overview of the main steps applied within the data processing pipeline is given in Figure B.1.

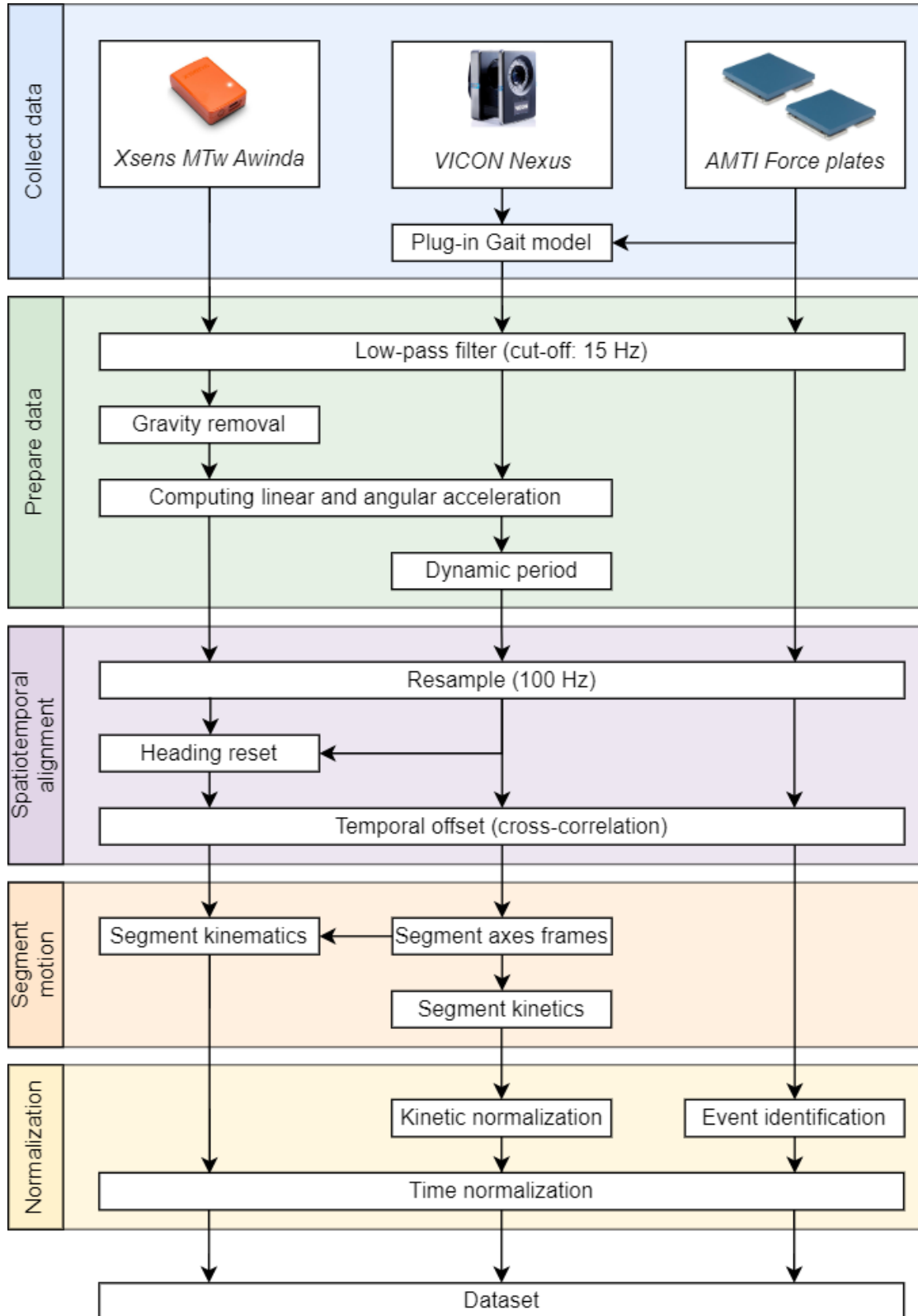


Figure B.1. Detailed overview of data processing steps applied to each trial.

A graphical user interface (GUI) was developed to give insight into the different spatial orientation of the sensors and segments. With this GUI, the steps concerning spatiotemporal alignment and segment motion could be checked. For instance, it was determined whether the heading reset was applied correctly, such that the sensor orientation was coincident with the global coordinate frame of the OMC system. This is presented in Figure B.2.

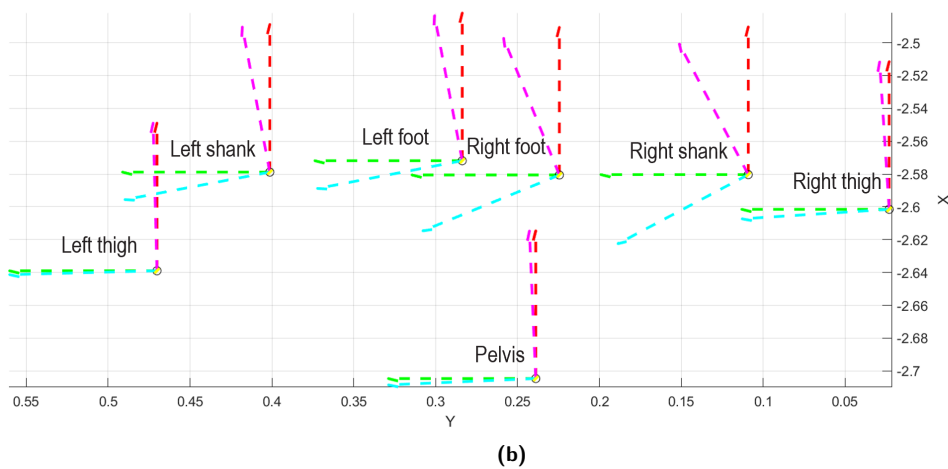
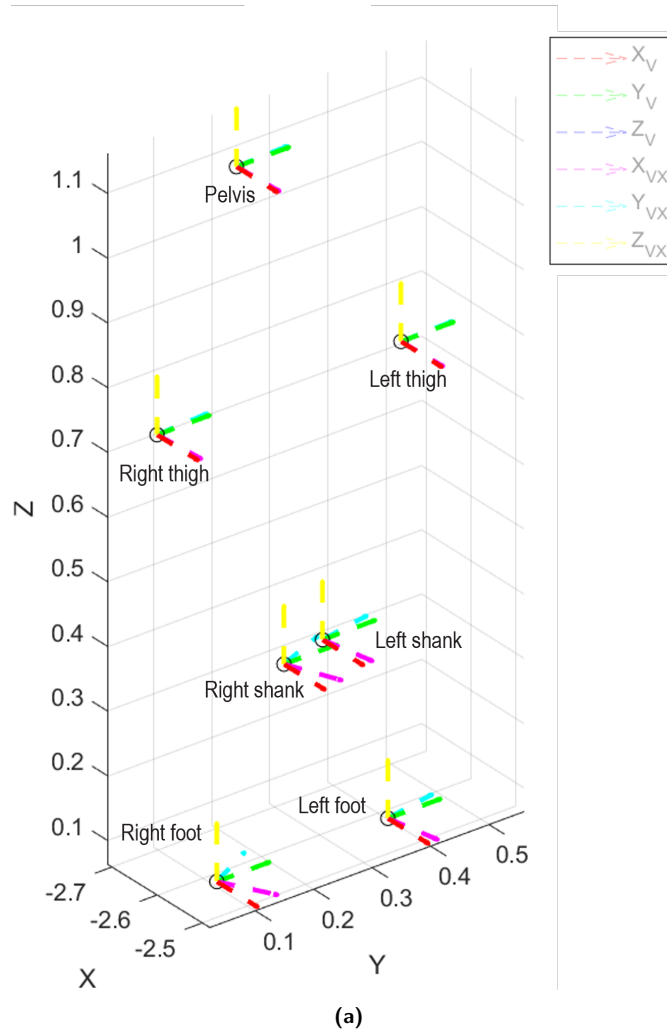


Figure B.2. Heading reset applied to the sensor data visualized in the developed GUI: oblique view at 45° (a) and transverse view (b).

To determine whether the IMC and OMC systems were temporally aligned, the data corresponding to the right thigh was used. A representative illustration is given in Figure B.3.

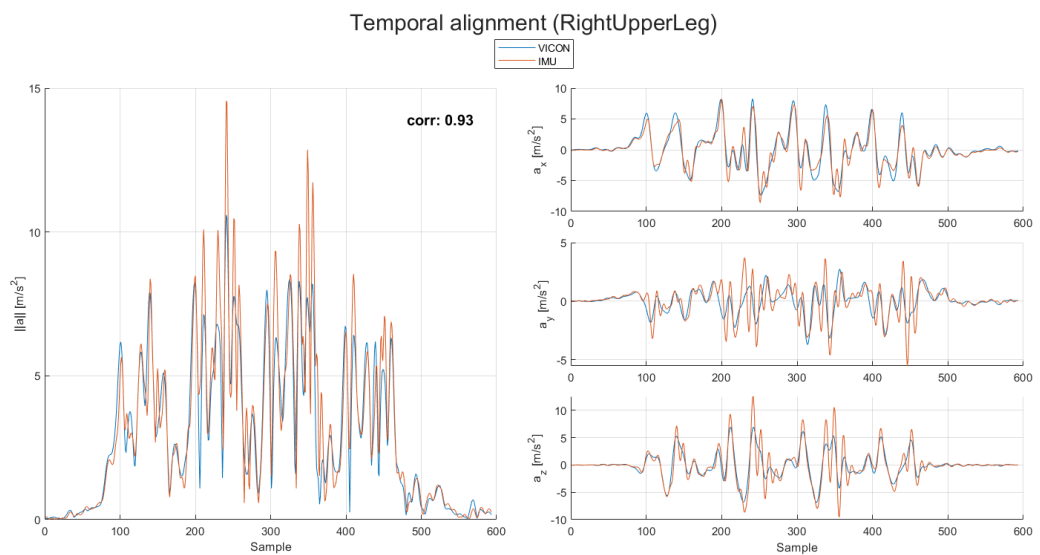
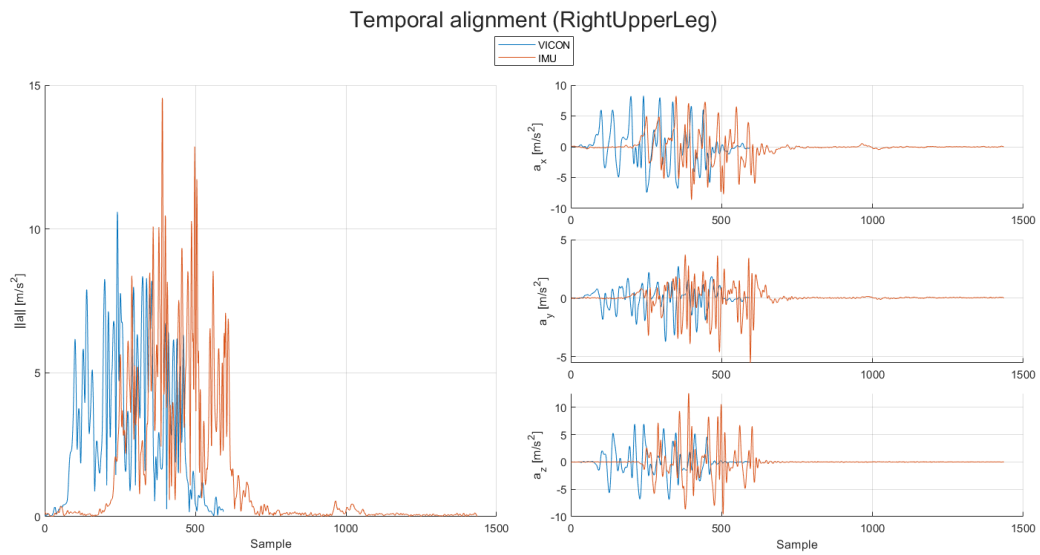


Figure B.3. Representative linear accelerations of the right thigh before (a) and after temporal alignment (b) of the IMC (IMU) and OMC (VICON) systems.

C Estimation performance per fold

Table C.1. Overview of Pearson's r and $rRMSE$ values for knee joint and ground reaction (GR) kinetics during walking. The table summarizes the performance of the PINN and baseline FNN models, evaluated on the test-subject used in the cross-validation folds for healthy and injured cohorts.

			F_{AP}^*		F_{ML}^*		F_V^*		M_{ML}^*		M_{AP}^*		M_V^*	
			r	rRMSE [%BW]	r	rRMSE [%BW]	r	rRMSE [%BW]	r	rRMSE [%BW]	r	rRMSE [%BW]	r	rRMSE [%BW]
002	Knee	FNN	0.85	15.96	0.34	73.38	0.81	15.98	0.69	23.46	0.51	41.50	0.73	24.86
		PINN	0.79	18.73	0.25	84.09	0.64	24.33	0.57	33.10	0.59	45.50	0.67	28.15
	GR	FNN	0.67	26.49	0.96	9.96	0.79	17.25	0.82	43.09	0.70	23.67	0.90	12.63
		PINN	0.70	23.26	0.95	14.83	0.67	23.10	0.78	54.42	0.32	38.03	0.91	13.49
003	Knee	FNN	0.78	18.01	0.54	48.92	0.80	17.51	0.54	37.61	0.49	43.94	0.62	28.08
		PINN	0.86	15.84	0.57	59.78	0.79	19.05	0.52	31.25	0.64	42.64	0.87	19.76
	GR	FNN	0.42	31.90	0.90	15.27	0.79	18.19	0.81	20.15	-0.04	66.67	0.78	25.30
		PINN	0.64	22.71	0.89	18.88	0.80	18.47	0.91	24.60	0.49	51.75	0.90	24.50
004	Knee	FNN	0.85	17.61	0.34	79.44	0.80	19.66	0.66	25.22	0.12	81.25	0.58	40.20
		PINN	0.81	19.22	0.24	76.51	0.78	19.51	0.59	28.69	0.28	84.35	0.53	43.98
	GR	FNN	0.73	25.01	0.91	16.66	0.82	19.45	0.90	16.34	0.68	30.37	0.85	24.24
		PINN	0.75	22.80	0.82	19.44	0.81	19.86	0.82	21.00	0.71	28.35	0.83	24.68
007	Knee	FNN	0.88	24.08	0.35	67.02	0.85	17.14	0.64	33.88	0.25	65.04	0.52	40.46
		PINN	0.88	23.44	0.22	67.28	0.86	17.90	0.63	34.25	0.26	67.29	0.56	39.85
	GR	FNN	0.83	39.48	0.89	16.27	0.82	18.26	0.67	44.11	0.85	50.52	0.77	27.48
		PINN	0.85	40.13	0.90	16.96	0.85	18.20	0.66	43.05	0.79	49.51	0.78	28.37
008	Knee	FNN	0.66	22.13	0.34	59.23	0.73	19.17	0.64	27.44	0.41	49.11	0.82	29.14
		PINN	0.69	21.07	0.33	50.85	0.77	17.78	0.68	26.07	0.45	44.36	0.82	30.04
	GR	FNN	0.61	24.23	0.95	9.89	0.73	19.00	0.79	31.34	0.65	28.20	0.91	15.35
		PINN	0.61	24.36	0.95	10.36	0.74	18.74	0.74	33.66	0.65	27.84	0.89	16.15
009	Knee	FNN	0.86	14.38	0.42	37.40	0.81	18.56	0.67	24.48	0.57	30.89	0.72	28.95
		PINN	0.81	20.12	0.46	33.03	0.79	18.78	0.61	28.32	0.76	23.34	0.78	26.97
	GR	FNN	0.73	32.71	0.89	14.60	0.81	17.63	0.75	35.90	-0.24	91.82	0.52	38.81
		PINN	0.77	34.81	0.90	13.58	0.82	16.26	0.75	42.34	-0.15	82.50	0.57	31.60
P01	Knee	FNN	0.83	22.10	0.91	30.54	0.83	19.63	0.22	65.83	0.81	52.43	0.55	36.11
		PINN	0.72	23.20	0.57	70.02	0.85	15.63	0.76	52.95	0.65	40.92	0.26	49.50
	GR	FNN	0.86	34.09	0.83	29.55	0.84	20.29	0.45	43.69	0.76	51.77	0.84	50.84
		PINN	0.85	18.95	0.60	35.14	0.86	15.28	-0.08	70.68	0.74	28.44	0.57	49.27
P03	Knee	FNN	0.69	28.67	0.72	28.18	0.73	24.41	0.61	35.28	0.76	33.17	0.64	39.17
		PINN	0.77	38.68	0.26	39.08	0.74	23.28	0.63	23.98	0.69	25.93	0.64	39.65
	GR	FNN	0.75	24.95	0.69	28.91	0.75	22.26	0.70	41.90	0.56	30.07	0.48	34.22
		PINN	0.65	31.92	0.57	32.85	0.78	22.76	-0.46	69.77	0.44	37.72	0.40	37.51
P05	Knee	FNN	0.76	31.22	0.32	74.52	0.84	30.55	0.41	42.23	0.56	39.37	0.81	36.07
		PINN	0.86	18.29	0.77	43.16	0.95	11.55	0.73	23.96	0.75	24.75	0.93	17.25
	GR	FNN	0.51	43.56	0.86	32.00	0.78	30.95	0.65	57.58	0.67	40.01	0.83	31.00
		PINN	0.85	17.73	0.88	17.04	0.95	10.34	0.58	51.18	0.94	13.36	0.86	21.42
P06	Knee	FNN	0.78	30.55	0.20	102.44	0.66	27.71	0.29	33.72	0.70	58.61	0.46	46.32
		PINN	0.85	17.11	0.61	72.10	0.43	36.67	-0.35	51.71	0.24	53.49	0.57	31.00
	GR	FNN	0.76	41.48	0.88	22.60	0.69	28.32	0.74	28.55	-0.44	236.28	0.44	32.20
		PINN	0.59	32.15	0.76	20.64	0.56	31.76	-0.05	47.07	-0.45	99.63	0.37	44.03
P07	Knee	FNN	0.84	13.99	0.19	45.12	0.86	13.86	0.07	57.12	0.82	34.10	0.71	27.19
		PINN	0.76	18.37	0.76	22.24	0.79	16.98	0.14	55.83	0.40	34.29	0.33	42.22
	GR	FNN	0.58	23.91	0.92	14.52	0.89	12.30	0.39	99.37	0.32	36.85	0.88	14.95
		PINN	0.73	22.36	0.84	20.77	0.78	17.22	0.18	81.80	0.52	28.61	0.78	19.98

Table C.2. Overview of Pearson's r and $rRMSE$ values for knee joint and ground reaction (GR) kinetics during SLH. The table summarizes the performance of the PINN and baseline FNN models, evaluated on the test-subject used in the cross-validation folds for healthy and injured cohorts.

			F_{AP}^*		F_{ML}^*		F_V^*		M_{ML}^*		M_{AP}^*		M_V^*	
			r	rRMSE [%BW]	r	rRMSE [%BW]	r	rRMSE [%BW]	r	rRMSE [%BW]	r	rRMSE [%BW]	r	rRMSE [%BW]
002	Knee	FNN	0.94	6.52	0.28	42.98	0.95	6.64	0.83	9.67	0.16	30.96	0.41	36.11
		PINN	0.96	5.66	0.28	45.33	0.94	6.66	0.88	9.39	0.23	35.45	0.70	35.22
	GR	FNN	0.36	16.52	0.89	8.01	0.96	5.41	0.48	22.86	0.20	42.56	0.22	37.28
		PINN	0.55	17.14	0.87	9.61	0.96	5.20	0.47	23.30	0.55	47.97	0.58	40.68
003	Knee	FNN	0.87	10.66	0.69	28.03	0.90	9.42	0.80	12.57	0.73	23.97	0.49	22.85
		PINN	0.88	9.40	0.54	28.54	0.91	9.10	0.84	11.52	0.54	23.46	0.51	21.32
	GR	FNN	0.47	17.16	0.78	12.40	0.91	9.32	0.48	26.97	0.35	43.11	0.24	20.75
		PINN	0.51	17.70	0.76	13.50	0.92	8.67	0.38	32.24	0.32	40.82	0.35	19.80
004	Knee	FNN	0.85	14.05	0.37	44.04	0.84	11.80	0.69	17.36	0.23	46.58	0.20	50.65
		PINN	0.80	15.06	0.35	48.62	0.77	13.45	0.66	18.12	0.10	50.85	0.05	57.75
	GR	FNN	0.45	22.61	0.78	13.69	0.85	11.24	0.65	29.76	0.26	63.54	0.10	33.08
		PINN	0.39	23.51	0.69	15.58	0.81	12.54	0.64	32.02	0.21	59.10	0.20	32.06
005	Knee	FNN	0.48	20.13	0.52	32.67	0.57	17.60	0.39	19.27	0.46	27.18	0.19	34.38
		PINN	0.40	21.17	0.35	29.73	0.43	19.82	0.34	19.50	0.36	25.39	0.03	33.54
	GR	FNN	0.26	24.89	0.68	16.14	0.55	18.42	0.28	36.45	0.25	36.01	0.40	31.21
		PINN	0.21	23.25	0.59	16.23	0.44	19.76	0.25	33.88	0.13	43.63	0.37	30.02
006	Knee	FNN	0.89	8.75	0.75	24.30	0.92	7.44	0.76	14.33	0.69	28.62	0.40	29.66
		PINN	0.89	8.66	0.70	25.75	0.90	8.33	0.75	13.85	0.60	30.39	0.44	29.24
	GR	FNN	0.54	18.35	0.87	8.21	0.94	6.13	0.64	26.24	0.34	29.62	0.36	18.83
		PINN	0.52	19.29	0.85	9.07	0.93	6.95	0.72	23.85	0.27	34.95	0.28	18.14
007	Knee	FNN	0.83	12.73	0.57	23.68	0.89	8.45	0.66	19.55	0.58	22.73	0.47	30.87
		PINN	0.83	12.34	0.56	25.92	0.88	8.97	0.64	19.83	0.61	23.58	0.55	35.37
	GR	FNN	0.59	28.94	0.83	10.08	0.90	8.21	0.61	30.90	0.12	54.94	-0.05	26.70
		PINN	0.57	28.99	0.84	10.30	0.89	8.51	0.63	32.91	0.19	53.89	-0.07	27.79
008	Knee	FNN	0.86	9.13	0.55	20.53	0.89	8.79	0.66	16.26	0.48	25.24	0.27	45.53
		PINN	0.86	9.23	0.57	20.51	0.90	8.45	0.64	17.81	0.49	23.94	0.24	56.48
	GR	FNN	0.49	18.30	0.76	10.37	0.90	8.08	0.23	23.48	0.41	54.60	0.25	29.20
		PINN	0.45	19.20	0.76	11.41	0.90	8.03	0.29	24.45	0.35	52.11	0.19	32.96
009	Knee	FNN	0.85	9.82	0.61	16.25	0.84	10.76	0.76	12.43	0.51	20.17	0.27	23.63
		PINN	0.82	11.73	0.70	15.06	0.74	14.27	0.78	13.22	0.61	19.45	0.27	28.60
	GR	FNN	0.24	28.17	0.83	10.90	0.86	9.59	0.27	24.05	0.07	35.47	0.30	23.46
		PINN	0.26	31.09	0.83	12.26	0.78	12.82	0.33	25.00	0.09	43.28	0.11	27.19
P01	Knee	FNN	0.61	21.85	0.47	25.20	0.63	15.99	0.32	28.12	0.25	27.77	0.25	28.62
		PINN	0.64	21.39	0.59	24.05	0.66	14.42	0.36	28.26	0.29	26.87	0.21	28.55
	GR	FNN	-0.10	28.72	0.04	25.44	0.66	16.37	0.48	31.15	0.15	53.76	-0.07	37.48
		PINN	-0.06	28.87	-0.01	26.69	0.67	15.53	0.40	30.78	0.18	54.13	-0.09	37.65
P03	Knee	FNN	0.69	17.10	0.65	16.41	0.85	13.31	0.63	17.02	0.59	19.47	0.25	30.41
		PINN	0.75	15.17	-0.07	21.60	0.86	10.84	0.63	17.60	0.18	24.76	0.33	24.06
	GR	FNN	0.27	24.64	0.33	27.27	0.85	11.57	0.35	45.72	0.42	49.60	0.24	26.33
		PINN	0.30	17.06	-0.59	29.38	0.85	11.49	0.22	29.36	0.30	23.79	-0.39	26.19
P05	Knee	FNN	0.65	21.01	0.82	33.27	0.78	12.79	0.64	24.51	0.77	27.97	0.41	22.10
		PINN	0.68	20.71	0.76	36.09	0.76	14.12	0.70	21.88	0.74	27.38	0.53	20.81
	GR	FNN	0.43	17.72	0.45	17.58	0.80	12.81	0.37	32.57	0.51	30.98	0.26	20.95
		PINN	0.34	19.05	0.40	21.24	0.76	14.60	0.32	33.27	0.33	30.07	0.11	22.93
P06	Knee	FNN	0.81	13.49	-0.40	62.53	0.89	12.04	0.69	16.44	-0.14	51.67	0.53	35.47
		PINN	0.80	13.94	-0.54	66.85	0.87	10.30	0.73	15.71	-0.07	48.31	0.51	32.45
	GR	FNN	0.05	41.93	0.09	24.78	0.89	11.28	0.32	61.16	0.10	79.76	-0.28	51.95
		PINN	0.34	43.25	0.63	19.77	0.93	9.96	0.31	59.68	-0.08	75.72	-0.32	51.38
P07	Knee	FNN	0.75	13.74	0.64	27.74	0.85	11.63	0.18	44.66	0.57	19.01	0.40	30.55
		PINN	0.73	12.73	0.58	43.02	0.84	12.08	0.11	39.82	0.57	20.01	0.38	27.46
	GR	FNN	0.27	29.19	-0.09	30.08	0.85	11.26	0.05	50.87	0.38	46.90	-0.19	49.17
		PINN	0.09	27.05	-0.28	29.28	0.84	10.49	0.16	43.41	0.33	64.46	-0.18	51.39

D Target knee kinetics

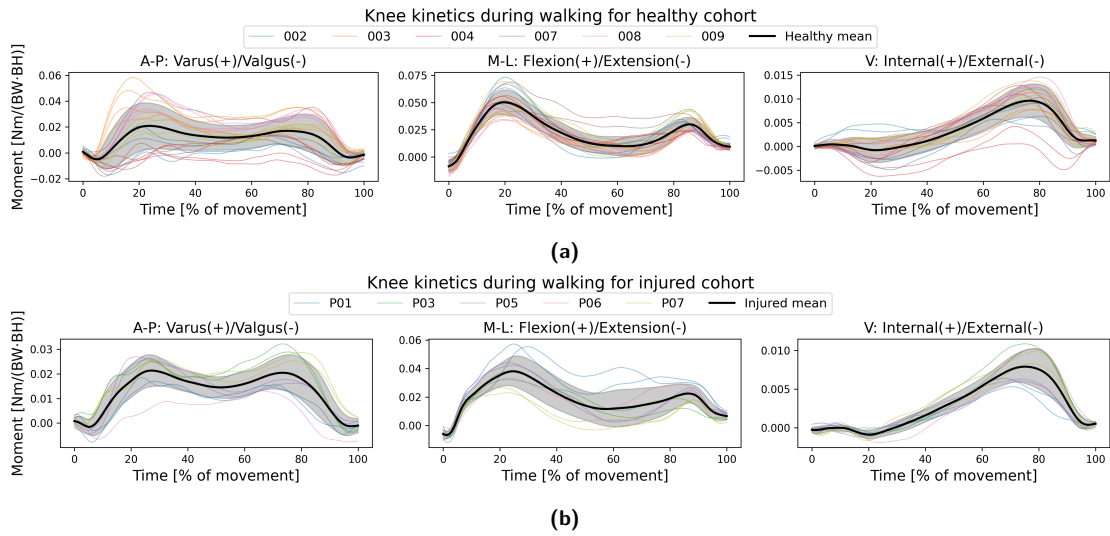


Figure D.4. Individual KJM trajectories corresponding to subjects (subject number) and mean across subjects during walking for the healthy cohort (a) and injured cohort (b). Individual trajectories (colored lines), and cohort mean (black line) and SD (black shaded area).

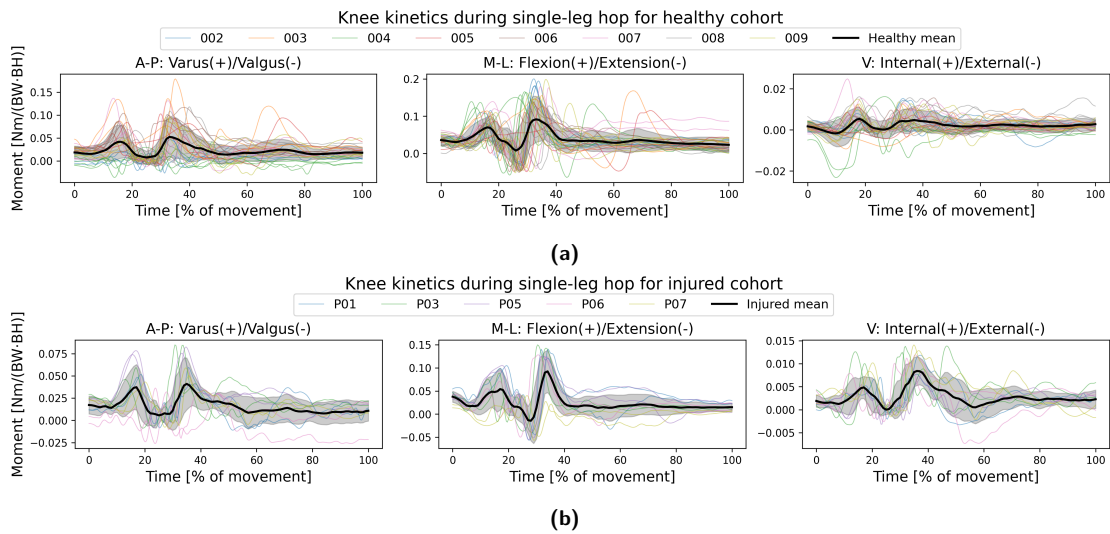


Figure D.5. Individual KJM trajectories corresponding to subjects (subject number) and mean across subjects during SLH for the healthy cohort (a) and injured cohort (b). Individual mean (colored line) and SD (shaded area), as well as cohort mean (black line) are shown.

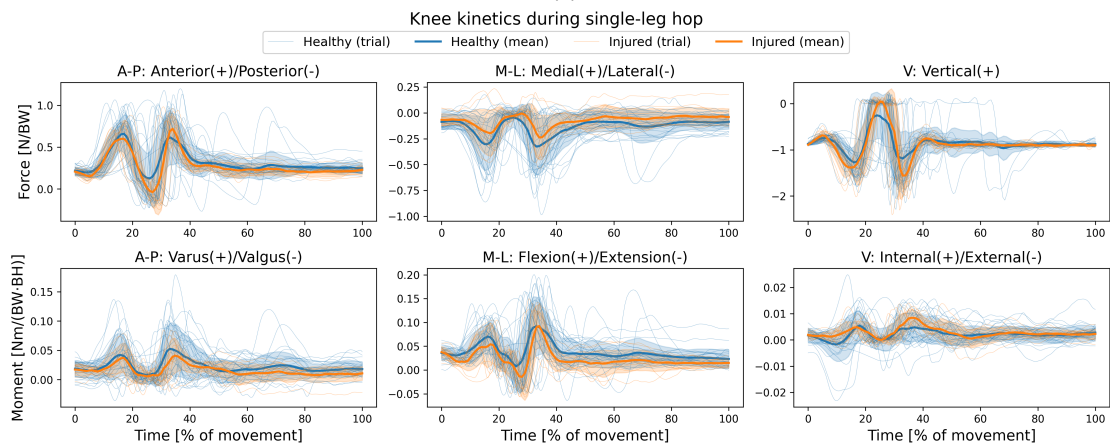
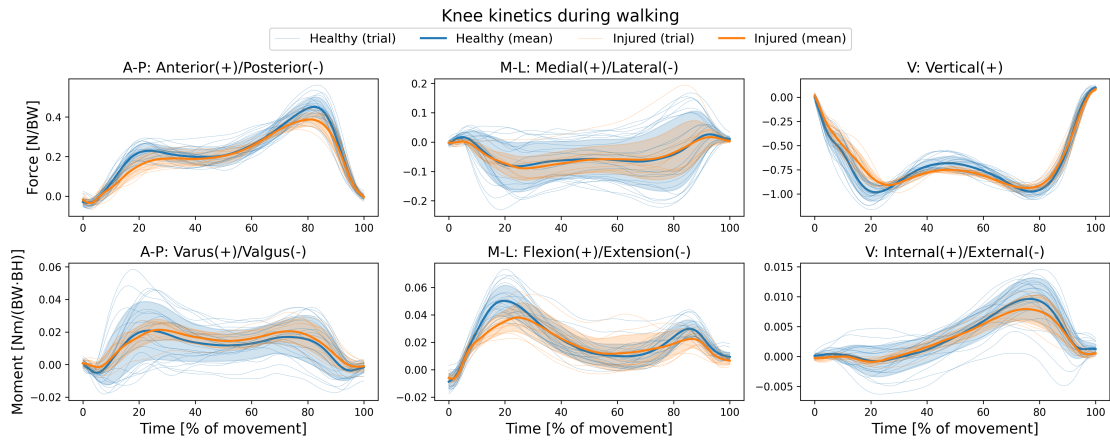


Figure D.6. Knee joint kinetic trajectories across trials during walking (a) and SLH (b) for healthy (blue) and injured (orange) cohort. Individual trials (thin line), cohort mean (bold line) and SD (shaded area) are shown.

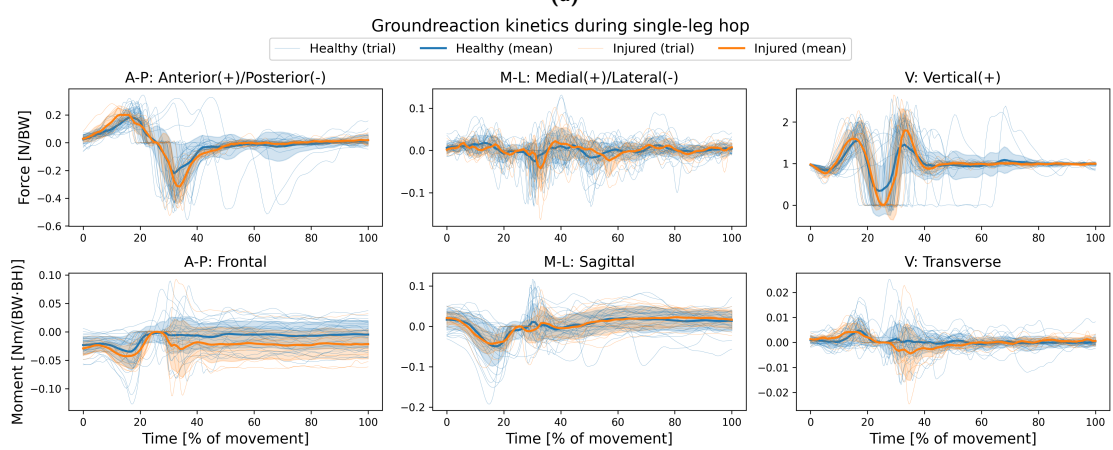
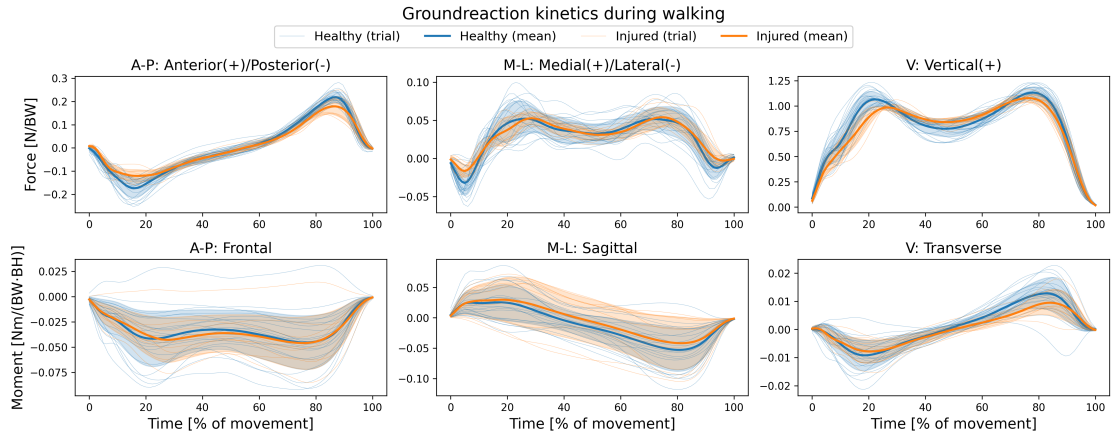


Figure D.7. Ground reaction kinetic trajectories across trials during walking (a) and SLH (b) for healthy (blue) and injured (orange) cohort. Individual trials (thin line), cohort mean (bold line) and SD (shaded area) are shown.

E Evaluation of input variables

Figure E.8 and Figure E.9 show the contribution of the kinematic input variables in both healthy and injured cohorts during walking and SLH, respectively.

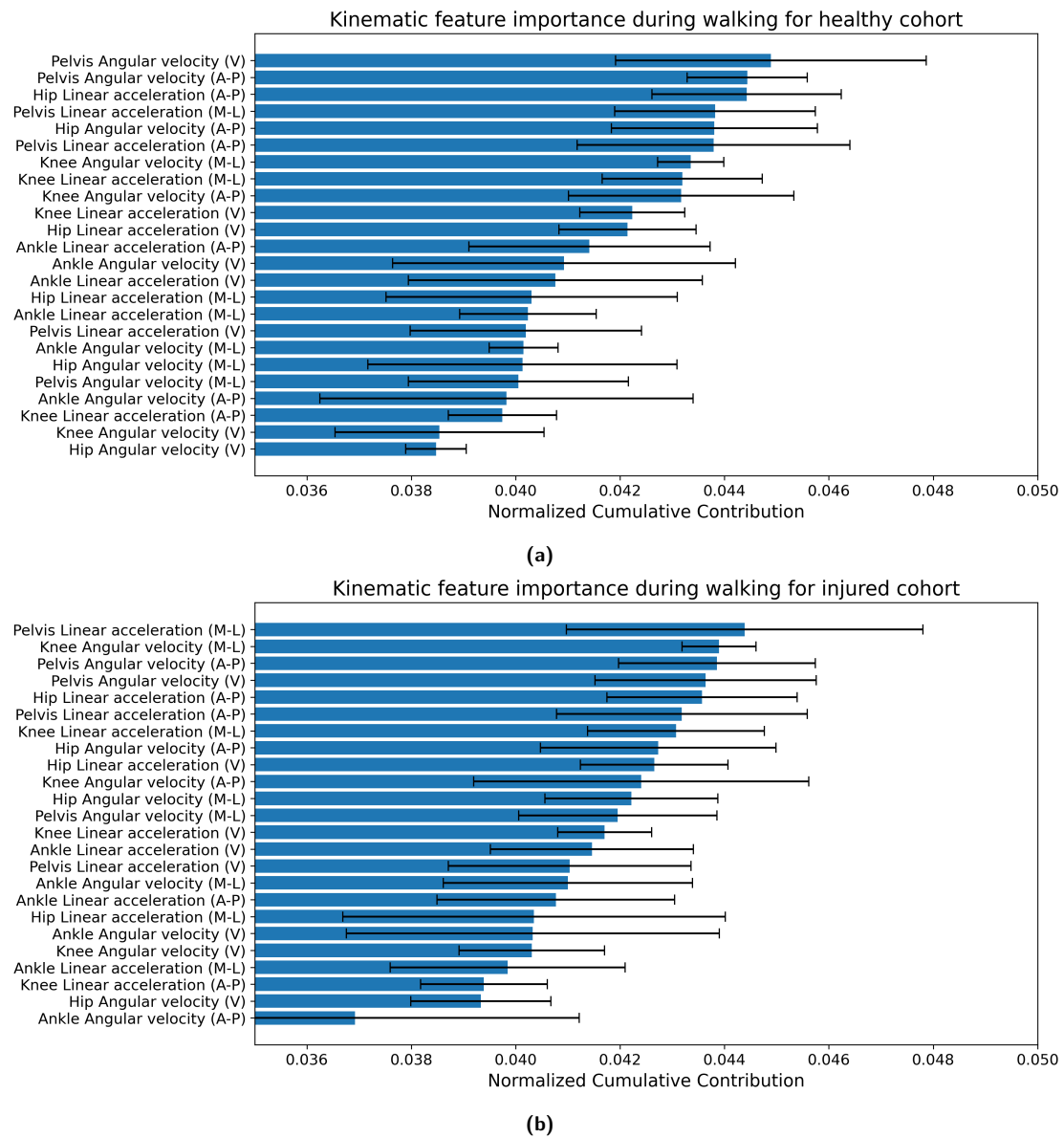
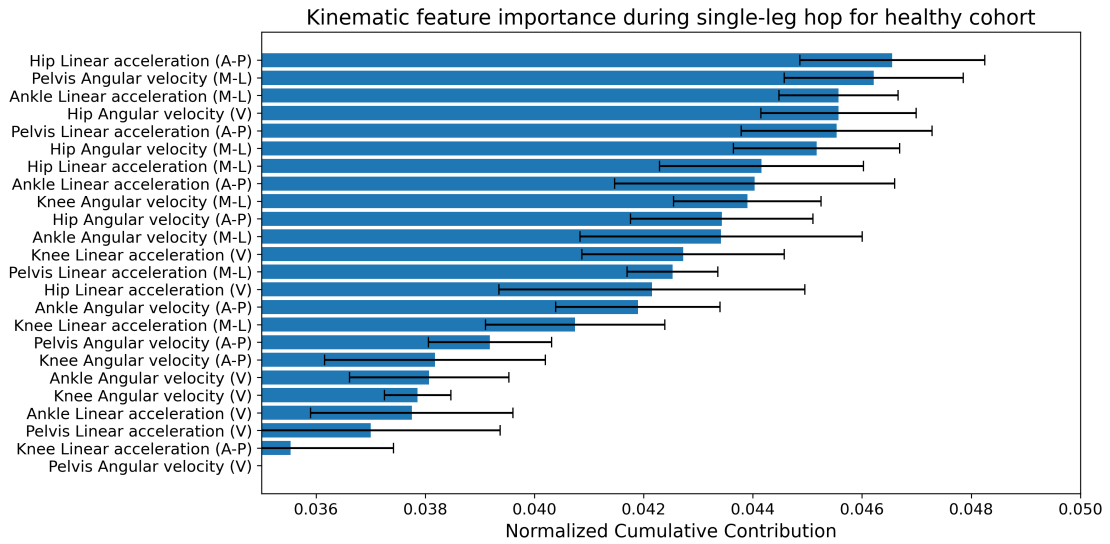
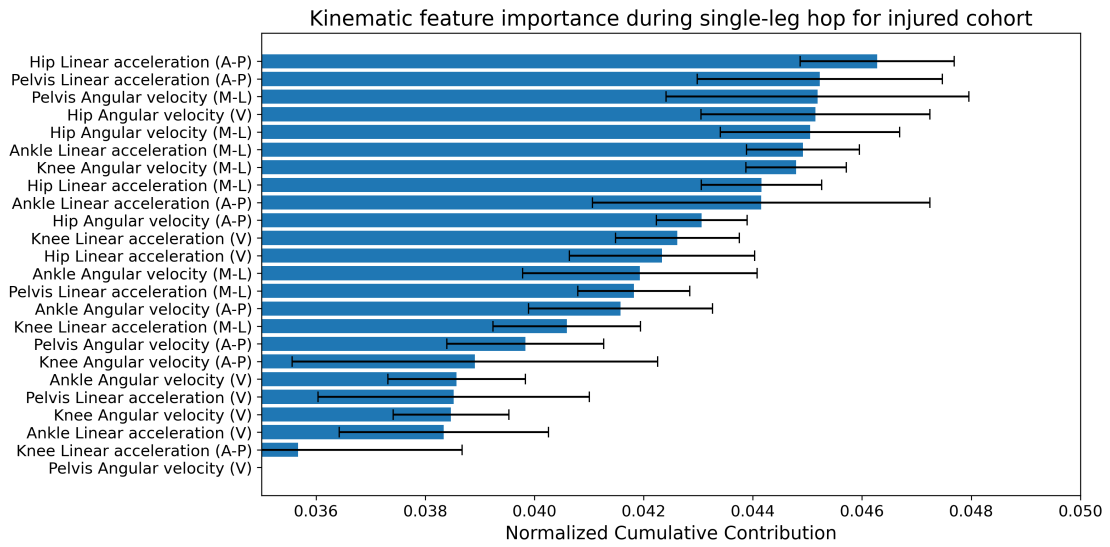


Figure E.8. Kinematic feature importance during walking for healthy (a) and injured (b) cohorts. Mean and SD across cross-validation folds are shown.



(a)



(b)

Figure E.9. Kinematic feature importance during SLH for healthy (a) and injured (b) cohorts. Mean and SD across cross-validation folds are shown.